Single cell transcriptome analysis of cavernous tissues reveals the key roles of pericytes in diabetic erectile dysfunction

Seo-Gyeong Bae[1†], Guo Nan Yin[2†], Jiyeon Ock[2†], Jun-Kyu Suh[2*], Ji-Kan Ryu[2,3*], Jihwan Park[1*]

[1]School of Life Sciences, Gwangju Institute of Science and Technology (GIST), Gwangju, Korea

[2]National Research Center for Sexual Medicine and Department of Urology, Inha University School of Medicine, Incheon, Korea

[3]Program in Biomedical Science & Engineering, Inha University, Incheon, Korea

†These authors contributed equally to this work.

*Corresponding authors

Jun-Kyu Suh, MD, PhD

National Research Center for Sexual Medicine and Department of Urology, Inha University School of Medicine

100 Inha-ro, Michuhol-gu, Incheon, Republic of Korea, 22212

E-mail: jksuh@inha.ac.kr

Ji-Kan Ryu, MD, PhD

National Research Center for Sexual Medicine and Department of Urology, Inha University School of Medicine

100 Inha-ro, Michuhol-gu, Incheon, Republic of Korea, 22212

E-mail: rjk0929@inha.ac.kr

Jihwan Park, PhD

School of Life Sciences, Gwangju Institute of Science and Technology

123 Cheomdangwagi-ro, Buk-gu, Gwangju, Republic of Korea, 61005

Tel: +82-62-715-2503 Fax: +82-62-715-2484 E-mail: jihwan.park@gist.ac.kr

Abstract

Erectile dysfunction (ED) affects a significant proportion of men aged 40–70 and is caused by cavernous tissue dysfunction. Presently, the most common treatment for ED is phosphodiesterase 5 inhibitors; however, this is less effective in patients with severe vascular disease such as diabetic ED. Therefore, there is a need for development of new treatment, which requires a better understanding of the cavernous microenvironment and cell-cell communications under diabetic condition. Pericytes are vital in penile erection; however, their dysfunction due to diabetes remains unclear. In this study, we performed single-cell RNA sequencing to understand the cellular landscape of cavernous tissues and cell type-specific transcriptional changes in diabetic ED. We found a decreased expression of genes associated with collagen or extracellular matrix organization and angiogenesis in diabetic fibroblasts, chondrocytes, myofibroblasts, valve-related lymphatic endothelial cells, and pericytes. Moreover, the newly identified pericyte-specific marker, Limb-bud and Heart (Lbh), in mouse and human cavernous tissues, clearly distinguishing pericytes from smooth muscle cells. Cell–cell interaction analysis revealed that pericytes are involved in angiogenesis, adhesion, and migration by communicating with other cell types in the corpus cavernosum; however, these interactions were highly reduced under diabetic conditions. Lbh expression is low in diabetic pericytes, and overexpression of LBH prevents erectile function by regulating neurovascular regeneration. Furthermore, the LBH-interacting proteins (Crystallin Alpha B and Vimentin) were identified in mouse cavernous pericytes through LC-MS/MS analysis, indicating that their interactions were critical for maintaining pericyte function. Thus, our study reveals novel targets and insights into the pathogenesis of ED in patients with diabetes.

Keywords: diabetes; erectile dysfunction; pericyte; single-cell RNA sequencing

Impact statement:

Single-cell RNA sequencing analysis of diabetic mouse cavernous tissue revealed that LBH as a novel pericyte marker and may interact with Crystallin Alpha B and Vimentin to promote neurovascular regeneration.

Introduction

Erectile dysfunction (ED) is an age-dependent vascular disease, affecting 5–35% of men aged 40–70 in varying degrees (Kubin et al., 2003). Although not fatal, 322 million men worldwide will be affected by the disease by 2025 (Ayta et al., 1999, Kessler et al., 2019). Moreover, it occurs in up to 75% of diabetes cases (Sáenz de Tejada et al., 2002). This causes significant physical and psychological problems for patients and their families (Bivalacqua et al., 2003). Moreover, the cavernous tissue is more prone to this disease than other blood vessels; therefore, its malfunction is considered as a biomarker in the progression of cardiovascular and vascular diseases (Miner, 2011). Current ED treatment involves the use of phosphodiesterase 5 (PDE5) inhibitors, but patients with severe vascular disease, such as diabetic ED, are less responsive. This is mainly because severe vascular dysfunction caused by diabetes results in insufficient bioavailable nitric oxide (NO) for PDE5 inhibitors to induce penile erection (Angulo et al., 2010). Therefore, it is necessary to identify novel therapeutic targets, which requires a comprehensive understanding of the cavernous microenvironment, including cell–cell interactions, regulatory signals, and molecular regulation. Although recent studies have proposed gene expression profiles of primary cultured cavernous cells exposed to hyperglycemic conditions (Anita et al., 2022, Ghatak et al., 2022, Yin et al., 2021), the relevant cell-specific relationships and genetic mechanisms in cavernous tissues have not been elucidated yet.

Pericytes are vital in the pathogenesis of erectile function as their interactions with endothelial cells are essential for penile erection. Pericytes interact with various cell types (especially endothelial cells) and are involved in angiogenesis, vasoconstriction, and permeability (Bergers and Song, 2005, Gerhardt and Betsholtz, 2003). Diabetes causes pericyte loss or dysfunction, thereby creating an imbalance between pericytes and endothelial cells, leading to vascular diseases (Liu et al., 2021, Warmke et al., 2016). For example, diabetic retinopathy is characterized by pericyte loss, capillary basement membrane thickening, and increased permeability, leading to retinal hypoxia and inflammation. Pericytes are particularly sensitive to glucose oxidation, which further promotes pericyte apoptosis (Warmke et al., 2016). Advanced glycation end products (AGEs) accumulate in pericytes under hyperglycemic conditions, thereby stimulating the secretion of transforming growth factor beta (TGFβ) in peripheral nerve pericytes, leading to basement membrane thickening, neovascularization, and pericyte apoptosis (Shimizu et al., 2011). Furthermore, our previous studies showed that restoring the content and function of cavernous pericytes significantly reduced the permeability of cavernous blood vessels and enhanced neurovascular regeneration (Yin et al., 2015, Yin et al., 2020, Yin et al., 2021). However, the

mechanisms underlying the effect of diabetes on pericyte dysfunction in the ED remain unclear.

Smooth muscle cells are also a vital component of the cavernous tissues in penile erection. Diabetes mellitus leads to smooth muscle cell dysfunction, such as decreased cavernosal smooth muscle relaxation, resulting in an inability to obtain or maintain satisfactory erection (Reddy et al., 2016, Wei et al., 2012). Since the marker genes of pericytes and smooth muscle cells often overlap, and their expression patterns are tissue-specific, identifying suitable *in vivo* markers to accurately interpret transcriptional and phenotypic changes in these cell types is of utmost importance (Chasseigneaux et al., 2018, Kumar et al., 2017, Smyth et al., 2018). Recent studies have identified pericyte-specific markers in different tissues using single-cell RNA sequencing (Baek et al., 2022, Sun et al., 2022), enabling characterization of various cell types and their cell–cell communication. In this study, a single-cell transcriptome analysis was performed to examine the cellular heterogeneity in erectile dysfunction caused by diabetes. The goal of this study was to identify markers specific to cavernous pericytes and understand their role in ED by exploring their interactions with other cell types.

Results

Single cell transcriptional landscape of mouse cavernous tissue

To elucidate the cellular landscape of mouse cavernous tissue and transcriptional changes in diabetic ED at the cellular level, we conducted a single-cell transcriptome analysis, profiling 12,894 cells **(Fig. 1A)**. The cells were grouped into 15 clusters based on their transcriptomic patterns, and cell types were annotated based on the expression of marker genes **(Fig. 1B, C)**. Clustering analysis identified fibroblasts (FB), chondrocytes (Chond), myofibroblasts (Myo-FB), lymphatic endothelial cells (LEC), valve-related LEC, vascular endothelial cells (VEC), smooth muscle cells (SMC), pericytes, Schwann cells, and macrophages. The Chond and FB subsets were further annotated with additional marker genes **(Fig. 1D, E, and Supplementary Fig. 1).**

Furthermore, we analyzed cell type-specific transcriptional changes due to diabetes **(Fig. 1F and Supplementary Fig. 2A-G)**. We found that *Nos3* (highly expressed in the untreated diabetes group compared to the treatment group) decreased in diabetic valve-related LEC and VEC (Ismail et al., 2020). In addition, *Igfbp2* and *Igfbp4* (lowly expressed in the penis of diabetic rats) were also downregulated in diabetic SMC and chondrocytes, respectively, whereas *Igfbp3* was upregulated in diabetic FB and Myo-FB (Abdelbaky et al., 1998). Collagen genes (vital in the corpus cavernosum structure) were significantly under expressed in diabetic FB, Chond, My-FB, and pericytes than in normal tissues (Sullivan et al., 2005). Gene ontology analysis using differentially expressed genes (DEGs) indicated that the genes associated with collagen or extracellular matrix organization and angiogenesis were downregulated in diabetic FB, Chonds, Myo-FBs, valve-related LEC, and pericytes compared to the cells under normal conditions **(Fig. 1G and Supplementary Fig. 3)**. In contrast, diabetic mice showed an increase in ribosome- and translation-related terms **(Fig. 1H and Supplementary Fig. 4)**. In Schwann cells, there were no significant DEGs between diabetic and normal cells.

Identifying specific markers for pericytes in mouse cavernosum tissues

We distinguished SMC from pericytes by examining the expression of previously known marker genes (*Cnn1*, *Acta2*, *Myh11*, *Tagln*, and *Actg2* for SMC, *Rgs5*, *Pdgfrb*, *Cspg4*, *Kcnj8*, *Higd1b*, and *Cox4i2* for pericytes) **(Fig. 2A and Supplementary Fig. 5A)**. However, rather than being exclusively expressed in each cell type, known

marker genes were co-expressed in each cell type. To ensure proper annotation of SMC and pericytes, we identified the gene sets enriched in each cluster through gene set enrichment analysis (GSEA). We found that the gene sets matching pericyte and SMC functions were enriched in each cluster **(Fig. 2B)**. Gene sets related to the regulation of blood vessels and leukocytes were enriched in pericytes, whereas gene sets related to actin or muscles were enriched in SMC, suggesting that these clusters were properly annotated. In addition, we screened six genes (*Lbh, Ednra, Gpc3, Npy1r, Pln,* and *Atp1b2*) that were highly expressed in the pericyte cluster from the single-cell analysis results **(Fig. 2C and Supplementary Fig. 5B)**. When we calculate AUC scores for the markers, *Rgs5* had the highest AUC, but *Rgs5* was also expressed in SMCs in our data (**Fig. 2A and Supplementary Fig. 5C**). *Pln, Ednra, Gpc3,* and *Npy1r* also seemed to be candidate markers, but the literature search excluded these genes as they are also expressed in the SMCs of other tissues or different cell types (Guo et al., 2020, Haghighi et al., 2014, Kowalczyk et al., 2015, Wittrisch et al., 2020). *Atp1b2* was also excluded because its protein expression was detected in both mouse cavernous pericytes and aortic SMC using immunofluorescence (IF) staining (**Supplementary Fig. 5D)**. In the single-cell data, *Lbh* (Limb-bud and Heart) was more specific for pericytes than *Rgs5*, a well-known marker for distinguishing between SMC and pericytes **(Fig. 2A, C)**. IF staining showed that LBH was optimally expressed in mouse cavernous pericyte, whereas it was rarely expressed in the smooth muscle cell (SMC) of the aorta, consistent with our single-cell data **(Fig. 2D, and Supplementary Fig. 5E).** In the blood vessels of other organ such as the bladder, α-SMA-expressing smooth muscle cell or CD31-expressing endothelial cells were surrounded by Lbh-expressing pericytes but rarely overlap **(Fig. 2E)**. LBH expression was easily distinguishable from CD31 or α-SMA in mouse dorsal vein and dorsal artery tissues in penile tissue (**Fig. 2F, top panel**), and is more specific than traditional pericyte markers (PDGFRβ) (**Fig. 2G, bottom panel**). For instance, PDGFRβ is expressed in pericytes and other surrounding tissue cells (as indicated by arrows and dotted area).

Finally, we examined *Lbh* expression patterns in various mouse tissues using the mouse single-cell atlas (Tabula Muris), although endothelial and pericyte clusters were not subclustered in most tissues from Tabula Muris. To identify pericytes, we relied on the expression pattern of known marker genes (*Pecam1* for endothelial cells, *Rgs5, Pdgfrb,* and *Cspg4* for pericytes). *Lbh* was expressed in pericytes of the bladder, heart and aorta, kidney, and trachea but not as specifically in penile pericytes (**Supplementary Fig. 6A-D**). However, it is worth noting that other known pericyte markers were also did not exhibit exclusive expression in pericytes across all the tissues we analyzed. Therefore, in certain tissues, particularly in mouse penile tissues, *Lbh* may be a valuable

marker in conjunction with other established pericyte marker genes for distinguishing pericytes.

Interactions between pericyte and other cell types in diabetes versus normal

Pericytes regulate various physiological functions involving other cell types such as EC and SMC. We compared the cell–cell interactions between pericytes and other cell types based on ligand-receptor interactions in single-cell data from mouse cavernous tissues under normal and hyperglycemic conditions. In diabetes, angiogenesis-related interactions, including vascular endothelial growth factor (VEGF) and fibroblast growth factor (FGF), were reduced between pericytes and other cell types compared to those under normal conditions **(Fig. 3A-C)**. In addition, interactions related to neuronal survival, adhesion, migration, and proliferation decreased in diabetic mice, as opposed to an increase in BMP signaling-related interactions **(Supplementary Fig. 7 and Supplementary Fig. 8)**. In addition to cell–cell interactions, the overall gene sets associated with angiogenesis, adhesion, and cell migration in pericytes were downregulated under diabetic conditions **(Fig. 3D)**. We performed gene regulatory network analysis to compare the activities of transcription factors (TFs) in pericytes under diabetic and normal conditions. In normal pericytes, TFs promoting angiogenesis (*Klf5*, *Egr1*, *Lmo2*, *Junb*, and *Elk1*) were significantly more active than in diabetic pericytes **(Fig. 3E)**. In contrast, TFs that inhibit angiogenesis (*Ppard* and *Hoxd10*) were more active in diabetes. Experimental data indicated that the expression level of *Lmo2*, *Junb*, *Elk1*, and *Hoxd10* was higher (*Hoxd10*) or lower (*Lmo2*, *Junb*, *Elk1*) in diabetic pericytes compared to normal pericytes (**Supplementary Fig. 9**). Furthermore, using the proteome profiler mouse angiogenesis array, we tested 53 angiogenesis factors in cavernous tissue, among which the expression of OPN (Dai et al., 2009), CD105 (Browne et al., 2018), TSP-2 (Kyriakides et al., 2001), IGFBP2 (Li et al., 2020), and IGFBP9 (Lin et al., 2003) decreased under diabetic conditions, while MMP-3 (Abdul et al., 2023), Angiogenin (Neubauer-Geryk et al., 2012), and PF4 (Cella et al., 1986) increased **(Fig. 3F and Supplementary Table 1)**. MMP-3 expression in the neurovascular unit is enhanced under diabetic conditions, leading to vascular damage (Abdul et al., 2023). Thus, angiogenesis activity decreased in mouse cavernous pericytes (MCPs) under diabetic conditions.

LBH improves erectile function under diabetic conditions through enhanced neurovascular regeneration

LBH is vital in promoting angiogenesis in human glioma under hypoxic conditions (Jiang et al., 2019). We

performed IF staining for LBH and another pericyte marker (CD140b) in mouse cavernous tissues to explore the effect of LBH on erectile dysfunction. We found that LBH and CD140b expression significantly decreased in the pericytes under diabetic conditions compared to those in age-matched controls (**Fig. 4A, C**). In addition, we assessed the expression of LBH *in vitro* under diabetic conditions and found that its expression was significantly decreased compared to that under normal conditions in mouse cavernous pericytes (**Fig. 4B, D**). All IF staining results were confirmed by western blotting (**Fig. 4E, F**). In addition, we overexpressed LBH in diabetic mice by intracavernosal injection of lentiviruses containing an ORF mouse clone of *Lbh* and assessed erectile function two weeks later (**Supplementary Fig. 10**). During electrical stimulation, the ratios of maximal and total intracavernous pressure (ICP) to mean systolic blood pressure (MSBP) were significantly reduced in PBS- and lentivirus ORF control particle-treated diabetic mice compared to age-matched controls. However, LBH overexpression in diabetic mice significantly improved this erection parameter, reaching 84% of the control values (**Fig. 4G, H and Supplementary Table 2**). Moreover, IF staining for CD31 (an endothelial cell marker), NG2 (a pericyte marker), neurofilament-2000 (NF), and neuronal NOS (nNOS) revealed that LBH overexpression significantly improved the endothelial cell, pericyte, and neuronal cell contents in diabetic mice (**Fig. 4I-N**). These effects were achieved by inducing the survival cells in the cavernosum tissues (such as decreased apoptosis, increased proliferation, migration, and tube formation) and major pelvic ganglion (MPG) neurite sprouting under diabetic conditions (**Supplementary Fig. 11**). Thus, LBH is vital in promoting neurovascular regeneration under diabetic conditions.

Expression of LBH in human cavernous pericytes and its role in diabetic conditions

Using a previous single-cell transcriptomics data of the human corpus cavernosum (Zhao et al., 2022), we examined whether *LBH* is highly expressed in human cavernous pericytes and has a similar role in diabetic conditions **(Fig. 5A)**. Further clustering of an SMC cluster (marker: *ACTA2*) in the previous study identified three subclusters; ACTA2-expressing cluster as myofibroblasts (MFBs), *CNN1*-expressing cluster as SMCs, and *RGS5*- and *LBH*-expressing clusters as pericytes **(Fig. 5B and Supplementary Fig. 12A-B)**. Gene Ontology analysis using DEGs between these clusters identified terms related to pericyte function in *LBH*-expressing pericytes (angiogenesis and leukocyte migration) **(Fig. 5C)**. The newly identified pericyte marker, LBH is also a marker of pericytes in the human corpus cavernosum, and LBH expression was significantly reduced in human

cavernous tissues from patients with diabetes-induced ED compared to age-matched controls (**Fig. 5D, F**). Furthermore, LBH expression was significantly reduced in primary cultured human cavernous pericytes under diabetic conditions compared to normal glucose conditions (**Fig. 5E, G**).

LBH-interacting protein identification in mouse cavernous pericytes

We conducted LC-MS/MS analysis following the immunoprecipitation of LBH from mouse cavernous pericytes to further elucidate the LBH-mediated systematic network in mouse cavernous pericytes. In protein–protein interaction (PPI) databases, only CRYAB was experimentally confirmed to interact with LBH (Pourhaghighi et al., 2020). However, only the co-fractionation of LBH and CRYAB has been outlined, and direct binding between the two proteins has not been elucidated yet. We identified αB-crystallin (CRYAB) from band 1 and Vimentin (VIM) from band 2 and 3, co-immunoprecipitated with LBH, VIM, and CRYAB (**Fig. 6A, B**). Furthermore, double IF staining indicated that LBH co-localized with CRYAB and VIM in mouse cavernous tissues and MCPs (**Fig. 6C, D**). Thus, CRYAB and VIM are novel LBH-interacting proteins in mouse cavernous pericytes.

Based on the STRING and BioGrid databases, we reconstructed the PPI network of CRYAB, VIM, and LBH, and the primary and secondary interacting proteins of LBH **(Fig. 6E)**. To identify the molecular mechanisms underlying interactions of LBH, CRYAB, and VIM, we performed gene ontology analysis using proteins from the PPI network. We found that these proteins are mainly involved in neurogenesis, neuronal development, and the nervous system **(Fig. 6F)**. In addition, the proteins involved in 'angiogenesis' and 'response to estradiol' that are associated with pericyte activity were also included in this PPI network. Since the expression of LBH was decreased in the pericytes under diabetic conditions, we identified the expression level of angiogenesis and nerve system-related genes in diabetic pericytes using single-cell data. GSEA showed that gene sets related to angiogenesis and the nervous system were enriched in normal pericytes compared to diabetic pericytes **(Fig. 6G)**. Finally, we found that CRYAB expression significantly reduced *in vitro* and *in vivo* under diabetic conditions, whereas VIM expression significantly increased (**Fig. 6H, I**). This reveals that the expression of nervous system- and angiogenesis-related genes are downregulated as LBH decreases in pericytes under diabetic conditions, affecting the interacting molecules.

Discussion

DM is a major cause of ED, and poor long-term glycemic control can lead to nerve and blood vessel damage (Desai et al., 2023). Many studies have outlined angiogenic and neurotrophic factors, such as VEGF, Comp-Ang1, dickkopf2, leucine-rich alpha-2 glycoprotein 1 (LRG1), brain-derived neurotrophic factor (BDNF), and neurotrophin-3 (NT3) that been tested as therapeutic options for ED (Bennett et al., 2005, Burchardt et al., 2005, Hu et al., 2018, Jin et al., 2011, Yin et al., 2018, Yin et al., 2022). However, poor efficacy, side effects such as inflammation, and complex drug-protein engineering have limited their success in clinical trials. A more detailed understanding of the intercellular signaling mechanisms and microenvironment in the penis under physiological and pathological conditions are necessary to provide more effective therapeutic targets. We therefore employed single-cell RNA sequencing to dissect the complex transcriptional changes in various cell types in ED using a diabetes-induced ED mouse model, as diabetic ED accounts for 75% of ED patients (Sáenz de Tejada et al., 2002). Our findings from *in vivo* animal models and *in vitro* experiments were confirmed using human data and samples, enabling us to understand how the results from mouse models could be translated to humans and developed as novel treatment targets.

It is well known that ED is a complex neurovascular disease (Leung et al., 2004), but the mechanism by which diabetes causes ED is still unclear. Many studies have showed that type 1 diabetes induces ED through different physiological processes, such as affecting penile contraction and relaxation, immune inflammatory response, neuropathy, structural and functional disturbance of cavernous smooth muscle cells, and dysfunction of endothelial cells, fibroblasts and pericytes (Liu et al., 2023, Thorve et al., 2011, Yin et al., 2015). Although other major cell populations in penile tissue such as smooth muscle cells, endothelial cell, and fibroblasts have been extensively studied, pericytes have mainly been investigated in the context of the central nervous system (CNS). For example, in the CNS, pericytes are involved in maintaining the integrity of the brain's blood-brain barrier (BBB) (Ferland-McCollough et al., 2017), regulating blood flow at capillary junctions (Gonzales et al., 2020), and promoting neuroinflammatory processes (Brown et al., 2019), whose dysfunction is considered an important factor in the progression of vascular diseases such as Alzheimer's disease (Winkler et al., 2014). But little is known about the role of pericytes in penile tissue (De Leonardis et al., 2022, Souza et al., 2022, Yin et al., 2015). In order to explore the role of pericytes in repairing the corpus cavernosum vascular and neural tissues damaged by DM, we focused on pericytes, which are multipotent perivascular cells that contribute to the

generation and repair of various tissues in response to injury (Birbrair et al., 2015). Although recent studies have shown that pericytes are involved in physiological mechanisms of erection, little is known about their detailed mechanisms. Many known pericyte markers are co-expressed in other cell types; thus, identifying the specific marker genes for pericytes *in vivo* is the first step characterizing pericyte cell type. From the pericyte cluster in the single-cell RNA sequencing results, we found that *Lbh, Ednra, Gpc3, Npy1r, Plm,* and *Atp1b2* are specific pericyte markers (**Supplementary Fig. 7**). LBH was identified as a pericyte-positive and SMC-negative marker that was also highly expressed in human cavernous pericytes (**Fig. 5**) and was validated through IF staining in many vascular tissues and cell types (**Fig. 2**). As it is widely known, peicytes are primarily located in capillaries, where they surround endothelial cells of blood vessels (Avolio and Madeddu, 2016). In our recent studies, we observed minimal overlap in staining between LBH and α-SMA and between LBH and CD31 in penile tissue (**Fig. 2, Supplementary Fig. 10A)**, suggesting that the cells expressing LBH were not smooth muscle cells or endothelial cells but possibly pericyte-like cells. In small vessels within the bladder, we also found that LBH-expressing cells surrounding CD31-expressing vessels and had minimal overlap with α-SMA-expressing smooth muscle cells, consistent with the known characteristics of pericytes. In addition, in the triple staining of CD31, LBH and α-SMA, we clearly found that LBH-expressing cells in the dorsal veins and dorsal artery showed LBH+/α-SMA-/CD31- staining (shown in Figure 2F). These results also indicate that the LBH-expressing cells and endothelial cell layer are completely distinct from the SMC layer. LBH-expressing cells are mostly distributed next to and outside endothelial cells. The distribution of LBH-expressing cells was similar to that of known pericytes. Further research is needed to comprehend the differences in LBH expression and its characteristics in other vascular tissues.

Lbh, a highly conserved transcription cofactor, is known to participate in early limb and heart development (Briegel and Joyner, 2001). Moreover, LBH can directly target the Wnt signaling pathway (Rieger et al., 2010) and regulate neural crest cell development (Powder et al., 2014). In addition, Jiang et al. showed that LBH overexpression promotes angiogenesis via VEGF-mediated ERK signaling (Jiang et al., 2019). In contrast, LBH inhibits cell migration and angiogenesis in nasopharyngeal carcinoma (Wu et al., 2022, Wu et al., 2021). These inconsistent results may be related to different histopathological environments. Thus, LBH has dual effects on the development of blood vessels and the nervous system, similar to other angioneurins such as VEGF and BDNF (Zacchigna et al., 2008). Here, we explored the role of Lbh in the penile tissues of diabetic mice. Interestingly, Lbh expression was significantly lower in cavernous pericytes in a diabetic mouse model.

Therefore, we hypothesized that the restoration of Lbh expression in the penis of diabetic mice will improve erectile function. To test our hypothesis, we utilized the diabetes-induced ED mouse model, commonly employed in various studies focusing on microvascular complications associated with type 1 diabetes. We observed that the overexpression of LBH in diabetic mice led to the restoration of reduced erectile function by enhancing neurovascular regeneration. However, this study primarily demonstrated the observed phenomenon without delving into the detailed mechanisms. In addition, our findings suggest that LBH can affect the function of cavernous pericytes, although we cannot definitively conclude which specific-cavernous cell types are affected by the overexpressed LBH, whether it be cavernous endothelial cells, smooth muscle cells, or others. Subsequent research will be required to conduct more comprehensive mechanistic investigations, such as *in vitro* studies using cavernous endothelial cells, smooth muscle cells, and fibroblasts to address these knowledge gaps. In summary, our results support the hypothesis that LBH can restores diabetes-induced ED by facilitating neurovascular regeneration (**Fig. 3**).

Previous studies have shown that CRYAB promotes angiogenesis (Dimberg et al., 2008) and interacts with LBH in nasopharyngeal carcinoma cells, where it enhances cell survival by inhibiting the autoproteolytic maturation of caspase-3 (Wu et al., 2021). Interestingly, our LC-MS/MS analysis of LBH following immunoprecipitation of MCPs identified VIM as a novel interaction partner and CRYAB (**Fig. 5**). In addition, we assessed the expression of CRYAB and VIM under diabetic conditions. Unexpectedly, the expression of VIM was increased, whereas that of CRYAB was downregulated in the penis of diabetic mice and MCPs under diabetic conditions. VIM is a type III intermediate filament protein expressed in mesenchymal cells (Dave and Bayless, 2014, Guo et al., 2013). It is involved in cell adhesion, migration, cellular integrity, epithelial-mesenchymal transition, and the malignant transformation and metastatic spread of cancer cells (Chen et al., 2021, Dave and Bayless, 2014, Liu et al., 2015). It is a multifunctional protein that interacts with several other proteins with many functions under various pathophysiological conditions (Danielsson et al., 2018). For example, VIM interacts with the insulin-like growth factor 1 receptor, promotes axonal extension, and serves as a double-edged sword in the nervous system by regulating axonal regeneration, myelination, apoptosis, and neuroinflammation (Chen et al., 2023). Furthermore, *VIM* knockout mice were less susceptible to bacterial infections and had a reduced inflammatory response than wild-type mice (Moisan et al., 2007). Recently, *VIM* deficiency was shown to prevent obesity and insulin resistance in type 2 DM by reducing CD36 expression on plasma membranes and intracellular trafficking of glucose transporter type 4 in adipocytes (Luo et al., 2021).

Therefore, the combination of LBH with CRYAB and VIM could improve neurovascular regeneration in diabetic ED by activating the angiogenic effects of CRYAB and potentially reducing the inflammatory effects of VIM. Collectively, the discovery of the LBH-CRYAB-VIM interaction opens the door to a more specific understanding of the role of pericytes in diabetic ED. However, the clinical implications of these results remain uncertain. Future research endeavors should focus on incorporating LBH-CRYAB-VIM into therapeutic strategies for diabetes and ED.

As far as our knowledge extends, this study marks the first demonstration of LBH's efficacy in restoring erectile function in mice with diabetes-induced ED. This not only introduces a novel approach to addressing diabetic ED but also carries substantial clinical relevance in mitigating other complications associated with diabetes.

Methods

Ethics statement and animal study design

Eight-week-old male C57BL/6 mice (Orient Bio, Seongnam-si, Gyeonggi-do, Korea) were used in this study. Animal experiments were approved by the Institutional Animal Care and Use Subcommittee of Inha university (approval number: 200910-719). Animals were monitored daily for health and behavior as previous studies described (Ghatak et al., 2022, Yin, 2022). Briefly, mice were maintained at room temperature (RT) (23 ± 2˚C), 40-60% relative humidity, 12 hours light/dark cycle, and specific pathogen-free conditions. Sixty adult male C57BL/6 mice were used for single cell sequencing analysis, mouse cavernous pericyte culture (*in vitro* study), and erectile function evaluation (*in vivo* study). All animals were anesthetized with intramuscular injections of ketamine (100 mg/kg, Yuhan Corp., Seoul, Korea) and xylazine (5 mg/kg, Bayer Korea, Seoul, Korea). Animals were euthanized by 100% CO_2 gas exchange in a closed container at a CO_2 exchange rate of 10-30% container volume/min. In this study, a total of 90 eight-week-old male C57BL/6 mice were used (10 for single cell RNA sequencing; 40 for mouse cavernous pericyte culture and related experiments; 20 for erectile function evaluated experiment; 20 for angiogenesis array and other fluorescence examinations.). Diabetes mellitus (DM) was induced as described previously (Jin et al., 2009). Shortly, low doses of streptozotocin (STZ, 50 mg/kg, i.p., Sigma-Aldrich, St. Louis, MO, USA) was injected for 5 consecutive days. Eight weeks later, only mice with a

tail vein blood glucose level higher than 300 mg/dL and significantly decreased body weights were considered to have DM. Fasting and postprandial blood glucose levels were determined using an Accu-Check blood glucose meter (Roche Diagnostics, Mannheim, Germany) before starting all *in vivo* studies. Body weights of STZ-treated (diabetic) mice were significantly lower than those of age-matched non-diabetic controls. Fasting and postprandial blood glucose concentrations were significantly higher in diabetic mice than in non-diabetic controls. However, diabetic mice infected with lentiviruses ORF control particles or lentiviruses containing ORF mouse clone of *Lbh* had no body weights and blood glucose levels change. Mean systolic blood pressures (MSBP) were similar in three STZ-treated groups and the non-diabetic control group (**Supplementary Table 2**). No mice died during erectile function evaluation experiment, and all experiments were performed in a blinded manner.

To test the efficacy of LBH on erectile function, the mice were distributed into four groups as follows: control nondiabetic mice (n = 5) and mice with STZ-induced diabetes receiving one successive intracavernous injections of phosphate-buffered saline (n = 5, PBS, 20 μL), lentiviruses ORF control particles (n = 5, NC, $5x10^4$ infection units in 20 μL; Origene Technology, Rockville, MD, USA) or lentiviruses containing ORF mouse clone of *Lbh*(n = 5, LBH O/E, $5x10^4$ infection units in 20 μL; Origene Technology) into the midportion of the corpus cavernosum. A vascular clamp was used to pressurize the bottom of penises immediately before injection and was left in place for 30 minutes to restrict blood outflow.

Single cell RNA sequencing

After mice were euthanized, the penis tissues (n = 5 for each group) were harvested, minced and digested using Multi Tissue dissociation kit (Miltenyi, 130-110-201) with minor modifications as described previously (Park et al., 2018). Due to the small size of mouse penile tissues, we pooled 5 corpus cavernosum tissues for each group. Briefly, tissues were homogenized using 21G and 26 1/2 G syringes. The tissues were digested with 50 μL of Enzyme D, 25 μL of Enzyme R and 6.75 μL of Enzyme A in 500 μL of DMEM and incubated for 10 minutes at 37 ˚C. The enzymes were deactivated by 10% FBS and solution was then passed through tip strainer (70 μm and then 40 μm). After centrifugation at 1,000 RPM for 5 minutes, cell pellet was incubated with 1 ml of RBC lysis buffer on ice for 3 minutes. After the cell number and viability were analyzed by using Countess AutoCounter (Invitrogen, C10227), the single cell suspension was loaded onto 10x Chromium Single Cell instrument (10x

Genomics). Barcoding and cDNA synthesis were performed according to the manufacturer's instructions.

Quality control, clustering, and cell type annotation

FASTQ files from sequencing were aligned to the mouse reference sequence (mm10) using CellRanger count pipeline (10x Genomics, Version 3.0.2). Filtered feature-barcode matrices outputs by CellRanger were used to create Seurat objects for single cell RNA sequencing data analysis (Seurat v3.1.5). Cells with the number of genes less than 200 were filtered out from Seurat objects. Quality controlled data were normalized using NormalizeData function with default parameters. Highly variable features were identified using the FindVariableFeatures function with default parameters. Data were scaled by setting the number of UMI as variables to regress out using ScaleData function. The scaled data were merged into one Seurat object, and then normalized, and highly variable genes were identified and scaled. Linear dimensional reduction performed using RunPCA function with 30 principal components. The RunHarmony function was used to correct the batch effect between the merged data. Cells were clustered based on similar feature expression patterns using FindClusters function (resolution = 1.5) and FindNeighbors (reduction = "harmony", dims = 1:20). To visualize and explore data, non-linear dimensional reduction was performed using Uniform Manifold Approximation and Projection (UMAP). To merge clusters with similar gene expression patterns, FindMarkers function (test.use = ‘bimod’) parameters was used to find differentially expressed genes (DEGs), and cluster pairs with less than 10 DEGs (adjusted p-value < 0.01, log_fold change ≥ 1) were merged. DEGs of each cluster were found using FindAllMarkers function (max.cells.per.ident = 100, min.diff.pct = 0.3, only.pos = TRUE).

The clusters were annotated by expression of marker genes (*Comp* and *Fn1* for Chondrocytes; *Col1a1*, *Col1a2* and *Fbln1* for Fibroblasts; *Mylk* and *Col3a1* for Fibrochondrocytes progenitor; *Prg4* and *Anxa8* for differentiating fibrochondrocyte; *Mgp* and *Mfap5* for reticular fibroblast; *C7*, *Lum* and *Mmp2* for Myofibroblast; *Prox1*, *Ccl21a* and *Lyve1* for Lymphatic endothelial cell; *Foxc2* for valve-related lymphatic endothelial cell; *Eng* and *Flt1* for vascular endothelial cell; *Cnn1*,*Acta2*, *Myh11*, *Tagln*, and *Actg2* for smooth muscle cell; *Rgs5*,*Cspg4*, and *Pdgfrb* for Pericyte; *Cadm4* and *Plp1* for Schwann cell; *Cd68*, *C1qa* and *C1qb* for Macrophage). The expressions of these marker genes were identified by FeaturePlot, VlnPlot, and FindAllMarkers function from Seurat package.

Identification of differential expressed genes and gene ontology analysis

DEGs between two groups were identified using FindMarkers function (test.use = ’MAST’) from Seurat R package. Among the DEGs found by FindMarkers based on bonferroni correction, only genes with |log_fold change| > 0.25 and adjusted p-value < 0.05 were considered as significant DEGs. DEGs were visualized as volcano plots. AUC scores of *Rgs5, Pln, Ednra, Npylr, Atp1b2,* and *Gpc3* for ability of a binary classifier to distinguish between pericyte and the other cell types in mouse penile tissues were measured by using FindMarkers function (test.use = ‘roc’). A pseudobulk DEG analysis for Lbh vs SMC or the other cell-types was performed by using FindMarkers function (test.use = ‘DESeq2). For the DESeq2 test, we added a pseudo-count of 1 to all read counts. Gene ontology analysis was performed using DAVID with significant DEGs as inputs. Gene ontology analysis on molecules of the protein-protein interaction network included parent terms (GOTERM_BP_5), and the others were gene ontology mappings directly annotated by the source database (GOTERM_BP_DIRECT). Only terms with p-value < 0.05 and FDR < 0.25 were considered significant gene ontology.

Gene set enrichment analysis (GSEA)

Enriched gene sets between two groups were identified using GSEA (http://www.broadinstitute.org/gsea/index.jsp) with 1000 gene set permutation. Curated (c2), ontology (c5) gene sets and hallmarks (h) gene sets were selected as gene sets database. A 'Signal2Noise' metric was used for ranking genes, and gene sets larger than 500 or smaller than 5 were excluded from the analysis. Only gene sets with p-value < 0.05 and false discovery rate < 0.25 were considered significant enriched gene sets.

Single cell data of Tabula Muris

To determine whether *Lbh* could also be a marker of pericyte in other tissues, we analyzed single cell RNA data from Tabula Muris (ref: https://doi.org/10.1038/s41586-018-0590-4). We downloaded and analyzed cell type annotated Seurat R objects. We used data from the microfluidic droplet method only. We subclustered pericytes from clusters annotated as endothelial cells by identifying the expression of known marker genes (*Pecam1* for endothelial cells, *Rgs5, Pdgfrb, Cspg4* for pericytes, *Rgs4* for heart pericytes, *Kcna5* for kidney pericytes). The expression of known marker genes and *Lbh* was confirmed through Seurat package’s FeaturePlot and VlnPlot function.

Single cell gene regulatory network analysis

Transcription factor (TF) activity of normal or diabetic pericyte were identified using SCENIC R package (v1.1.2-01). To avoid narrow comparison of TF activity in pericytes between normal and diabetic conditions that could lead to faulty reasoning, we included SMCs in the comparison as well. Raw count matrices of SMC and Pericyte extracted from the Seurat object were used as input for SCENIC. 10 kb around the transcription start site (TSS) and 500 bp upstream of the TSS were selected for motif ranking. Genes in input matrix were filtered using geneFiltering function with default parameters. To split targets into positive and negative correlated targets, the correlation was calculated using runCorrelation function. Potential transcription factor targets were inferred using runGenie3 function. Building and scoring the gene regulatory network were performed using runSCENIC functions. Clustering and dimensionality reduction on the regulon activity were performed using tsneAUC function. Only angiogenesis-related TFs with differences in activity between normal and diabetic pericytes were visualized in the heatmap. To assess differential regulon activities of transcription factors between diabetic pericytes and normal pericytes, we used generalized linear model using the scaled activity scores for each cell from SCENIC as input. We ran the generalized linear model using glm function in R programming.

Single cell data of human corpus cavernosum analysis

To determine whether *LBH* could also be a marker of pericyte in human, we analyzed single cell RNA data of human corpus cavernosum from previous study (Zhao et al., 2022). Quality control was performed according to method of previous study. Quality controlled data were processed according to our data analysis methods. Cells were clustered using FindClusters function (resolution = 0.5). The DEGs of three clusters expressing the SMC markers *ACTA2*, *MYH11*, and *ACTG2*, used in the previous study, were found with the FindAllMarker function. We defined significant DEGs as genes with log_fold change > 0.25, adjusted p-value < 0.05, and non-overlapping DEGs in different clusters. These significant DEGs were used for gene ontology analysis for cell type identification.

Cell-cell interaction analysis

Ligand-receptor communications between cell types were predicted using CellPhoneDB (https://github.com/Teichlab/cellphonedb) and CellChat (https://github.com/sqjin/CellChat). Normalized single

cell data was used as input for analysis. We performed CellPhoneDB with the statistical method. Interactions that did not differ by more than 0.25-fold mean values between diabetes and normal were considered to have no significant difference. Even if there is a difference in the mean value between diabetes and normal, interactions with p-value of 1 in both diabetes and normal were considered insignificant. The outputs of CellPhoneDB were visualized using ktplot in R. CellChat was performed according to tutorial for comparison analysis of multiple datasets with different cell type compositions. CellphoneDB permutes the cluster labels of all cells 1000 times and calculates the mean (mean (molecule 1 in cluster X), mean (molecule 2 in cluster Y)) at each time for each interaction pair, for each pairwise comparison between two cell types. We only considered interactions in which the difference in means calculated by these permutations were greater than 0.25-fold between diabetes and normal. Also, we considered that there is no interaction when the P-value is 1 and that the interactions with P-value < 0.05 were significant.

Protein-protein interaction (PPI) network visualization

PPIs of LBH, CRYAB, VIM, and 1st and 2nd interactors of LBH were found by BioGRID and STRING database (Organisms: Mus musculus). In the STRING database, textmining, experiments, and databases were used as active interaction sources, and only interactions with a minimum required interaction score higher than 0.7 were identified. The identified PPIs were visualized using Cytoscape (Shannon et al., 2003).

Cell culture

Mouse aortic smooth muscle cells (Aorta SMC; CRL-2797, ATCC) and human pericytes from placenta (hPC-PL; C-12980, PromoCell) were authenticated according to ATCC and PromoCell guidelines and used within 6 months of receipt. Aorta SMC and hPC-PL were cultured in complement Dulbecco's modified Eagle Medium (DMEM; Gibco, Carlsbad, CA, USA) supplemented with 10% FBS, and 1% penicillin/streptomycin (Gibco), and incubated the cells at 37°C in a 5% CO_2 atmosphere.

For the primary culture of mouse cavernous pericytes (MCPs), followed the protocol described previously (Neng et al., 2013, Yin et al., 2020), in brief, the cavernous tissue was cut into several pieces around 1 mm, and the pieces settled by gravity to the collagen I-coated 35-mm cell culture dishes (BD Biosciences). After 30 min incubation at 37°C with 300 µL complement of DMEM, 10% FBS, 1% penicillin/streptomycin, and 10 nM human pigment epithelium-derived factor (PEDF; Sigma- Aldrich), we added an additional 900 µL complement

medium and incubated the samples at 37℃ in a 5% CO2 atmosphere. Change the medium every 2 days. After the cells are confluent and spread to the bottom of the dish (approximately 2 weeks after the start of culture), subculture using only sprouting cells. The sprouting cells were seeded onto dishes coated with 50 μL/ml collagen I (Advanced BioMatrix). Cells between passages 2 and 4 were used for experiments. In order to examine the effect of LBH overexpression under normal glucose (NG, 5mM glucose, Sigma-Aldrich) or high glucose (HG, 30 mM glucose, Sigma-Aldrich) conditions, MCPs were infected with lentiviruses ORF control particles (NC, $5x10^5$ infection units per millilitre cultured medium; Origene Technology) or ORF clone of mouse *Lbh* (LBH O/E, $5x10^5$ infection units per millilitre cultured medium; Origen Technology) under high glucose conditions for at least 3 days.

Human corpus cavernosum tissue and cavernous pericyte culture

For fluorescence examinations, human corpus cavernosum tissues were obtained from two patients with congenital penile curvature (59-year-old and 47-year-old) who had normal erectile function during reconstructive penile surgery and two patients with diabetic ED (69-year-old and 56-year-old) during penile prosthesis implantation. For primary pericyte culture, the fresh adult corpus cavernosum tissues from patients (59-year-old) with congenital penile curvature who have normal erectile function during reconstructive penile surgery were collected after surgery and transferred into sterile vials containing Hank's balanced salt solution (GIBCO, Carlsbad, CA, USA) and washed twice in PBS. The detailed methods of the human cavernous pericytes were isolated and maintained as described previously (Neng et al., 2013, Yin et al., 2020). Human cavernous pericytes at passages 2 or 3 were used for experiments. All tissue donors provided informed consent, and the experiments were approved by the internal review board of our university.

RT-PCR

Total RNA was extracted from cultured cells using Trizol (Thermo Fisher Scientific) following the manufacturer's protocols. Reverse transcription was performed using 1 μg of RNA in 20 μl of reaction buffer with oligo dT primer and AccuPower RT Premix (Bioneer Inc., Daejeon, Korea). We used the following primers to measure relative changes in mRNA levels: mouse *Lmo2* forward, 5′-atccctgctgacatgtggtg-3′; mouse *Lmo2* reverse, 5′-cccagcttgtagtagaggcg-3′; mouse *Junb* forward, 5′-aggcagctacttttcgggtc-3′; mouse *Junb* reverse, 5′-ccagggctttgacaaaaccg-3′; mouse *Elk1* forward, 5′-gtagggatcaaacggtcacctt-3′; mouse *Elk1* reverse, 5′-

taaagacgtgtgcctctaccac-3′; mouse *Hoxd10* forward, 5′-agagtggcagaaagaagaggtg-3′; mouse *Hoxd10* reverse, 5′-cttgagtttcattcggcggttt-3′; *GAPDH* forward, 5′-ccactggcgtcttcaccac-3′; *GAPDH* reverse, 5′-cctgcttcaccaccttcttg-3′. The PCR reaction was performed with denaturation at 94°C for 30 s, annealing at 60°C for 30 s, and extension at 72°C for 1 minute in a DNA Engine Tetrad Peltier Thermal Cycler (MJ Research). For the analysis of PCR products, 10 µl of each PCR reaction was electrophoresed on 1% agarose gel and detected under ultraviolet light. GAPDH was used as an internal control.

Measurement of Erectile Function

Erectile function was measured after mice were anesthetized by intraperitoneal injection of ketamine (100 mg/kg) and xylazine (5 mg/kg) as described previously (Jin et al., 2009). Briefly, the cavernous nerve was stimulated for 1 minute using bipolar platinum wire electrodes at 1 or 5 V at 12 Hz and a pulse width of 1 ms condition. Each stimulation was repeated at least 2 times every 10 minutes. Record the maximal intracavernous pressure (ICP) and total ICP during stimulation. The area under the curve (AUC) from the initiation of cavernous nerve stimulation to 20 seconds after stimulation termination was measured as total ICP. Before ICP measurements, the systemic blood pressure was measured continuously using a noninvasive tail-cuff system (Visitech Systems, Apex, NC, USA). The ratio of maximal ICP and total ICP to mean systolic blood pressure (MSBP) was calculated to normalize variations in systemic blood pressure.

TUNEL Assay

The MCPs cell death after infected with lentiviruses ORF control particles (NC, $5x10^4$ infection units per millilitre cultured medium; Origene Technology) or ORF clone of mouse *Lbh* (LBH O/E, $5x10^4$ infection units per millilitre cultured medium; Origen Technology) under NG or HG conditions were evaluated by TUNEL (terminal deoxynucleotidyl transferase-mediated deoxyuridine triphosphate nick-end labeling) assay using the ApopTag® Fluorescein In Situ Apoptosis Detection Kit (S7160, Chemicon, Temecula, CA, USA) according to the manufacturer's instructions. Numbers of TUNEL-positive apoptotic cells were obtained by a confocal fluorescence microscope.

Cell migration assay

MCPs migration assays were performed using the SPLScar^{TM}Block system (SPL life sciences, Pocheon-si, Gyeonggi-do, Korea) on 60-mm culture dishes. In brief, MCPs was infected with lentiviruses ORF control particles (NC, $5x10^4$ infection units per millilitre cultured medium; Origene Technology) or ORF clone of mouse *Lbh* (LBH O/E, $5x10^4$ infection units per millilitre cultured medium; Origen Technology) under NG or HG conditions. Then conditioned cells were seeded into 3-well blocks at >90% confluence. Blocks were removed after 5 hours and cells were incubated for additional 24 hours in DMEM medium containing 2% FBS and thymidine (2 mM, Sigma-Aldrich). The images were taken using a phase-contrast microscope (Olympus), and cell migration was analyzed by determining the percentage of cells that moved into the frame line showed in the figures from four separate block systems in a blinded manner using Image J software (National Institutes of Health [NIH] 1.34, http://rsbweb.nih.gov/ij/).

***In vitro* tube formation assay**

Tube formation assay was performed as described previously (Yin, 2022). The assay was performed in a CO_2 incubator and the images were obtained at 24 hours with a screen magnification of 40 using a phase-contrast microscope (CKX41, Olympus, Japan). The numbers of master junctions from four separate experiments was determined by using Image J software.

***Ex vivo* neurite sprouting assay**

Major pelvic ganglion (MPG) tissues were harvested and maintained as described previously (Ghatak et al., 2022). After the tissue was covered with matrigel and incubated at 37 ℃ for 10 minutes in a 5% CO_2 atmosphere, followed by incubation in 1.2 ml of complete Neurobasal medium (Gibco) containing 0.5 nM GlutaMAX™-I (Gibco) and 2% serum-free B-27 (Gibco). The MPG tissues were infected with lentiviruses ORF control particles (NC, $5x10^4$ infection units per millilitre cultured medium; Origene Technology) or ORF clone of mouse *Lbh* (LBH O/E, $5x10^4$ infection units per millilitre cultured medium; Origen Technology) under NG or HG conditions. Five days later, neurite outgrowth segments were then fixed in 4% paraformaldehyde for at least 30 minutes and immunofluorescence staining with an anti-neurofilament antibody (N4142; Sigma-Aldrich; 1:50).

Proteome profiler Mouse angiogenesis array analysis

Secreted angiogenesis factors in cavernous tissue between normal and diabetes condition were detected using a proteome profiler mouse angiogenesis array kit (ARY015; R&D Systems Inc.), as described by the manufacturer. This array detects 53 mouse angiogenesis-related protein simultaneously. The intensity of dot blots was analyzed using Image J software. The criteria for selecting spots were an an expression density of at least 1500 and a change ratio greater than 1.2, as shown in the supplementary information.

Histological examination

For fluorescence examinations, tissues were fixed in 4% paraformaldehyde overnight at 4°C, and cell samples were fixed in 4% paraformaldehyde for 15 minutes at RT. After blocking with 1% BSA (Sigma-Aldrich) for 1 hour at RT, frozen tissue sections (12-μm as thick) or cell samples were incubated with primary antibodies at 4°C overnight. The antibodies used were as follows: anti-LBH (1:200; Novus Biologicals, Littleton, CO, USA), anti-CD31 antibody (1:50; Millipore), anti-PDGFR□ (1:100; Invitrogen), anti-α-SMA (1:100; Abcam, Cambridge, MA, USA), anti-CD140b (1:100; Invitrogen), anti-NG2 antibody (1:100; Millipore), anti-Neurofilament (1:100; Sigma-Aldrich), neuronal nitric oxide synthase (nNOS; 1:50; Santa Cruz Biotechnology, Dallas, TX, USA), anti-phospho-HistoneH3 (1:50; Millipore; 1:50), anti-Vimentin (1:100; Sigma-Aldrich), and anti-Crystallin Alpha B (CRYAB, 1:100; Invitrogen). Washes the samples with PBS (Gibco) for at least 3 times, tissue sections or cell samples were incubated with donkey anti-rabbit DyLight® 550 (1:200; Abcam), donkey anti-mouse Alexa Fluor® 488 (1:200; Jackson ImmunoResearch Laboratories, West grove, PA, USA), goat anti-Armenian hamster Fluorescein (FITC) (1:200; Jackson ImmunoResearch Laboratories), and donkey anti-chicken rhodamine (TRITC) secondary antibodies (1:200; Jackson ImmunoResearch Laboratories) for 2 hours at room temperature. Samples were mounted with a solution containing 4,6-diamidino-2-phenylindole (DAPI [H-1200, Vector Laboratories Inc., Burlingame, CA, USA]) for nuclei staining. All images were obtained using a confocal microscope (K1-Fluo; Nanoscope Systems, Inc.). Quantitative analysis was performed using Image J software (National Institutes of Health [NIH] 1.34, http://rsbweb.nih.gov/ij/).

LC-MS/MS analysis of immunoprecipitates

The LC-MS/MS analysis was performed as a custom service by Yonsei Proteome Research Center (Yonsei

Proteome Research Center, Seoul, Republic of Korea) as previously described (Yin et al., 2022). In brief, total cell lysates were immunoprecipitated with LBH antibody (1:50; Sigma-Aldrich), and analyzed by SDS-PAGE and Coomassie Blue staining. The indicated bands (**Fig. 6**, framed in red dot line) were excised from SDS-PAGE gels, and Nano LC-MS/MS analyses were performed using an Easy n-LC (Thermo Fisher, San Jose, CA, USA) and an LTQ Orbitrap XL mass spectrometer (Thermo Fisher) equipped with a nano-electrospray source (Lee et al., 2014). Samples were separated on a C18 nanobore column (150 mm × 0.1 mm, 3 μm pore size; Agilent). Mobile phase A for LC separation was 0.1% formic acid plus 3% acetonitrile in deionized water and mobile phase B was 0.1% formic acid in acetonitrile. The chromatography gradient was designed to achieve a linear increase from 0% B to 32% B in 23 minutes, 32% B to 60% B in 3 minutes, 95% B in 3 minutes, and 0% B in 6 minutes. The flow rate was maintained at 1500 nl/min. Mass spectra were acquired using data-dependent acquisition with a full mass scan (350–1800 m/z) followed by 10 MS/MS scans. For MS1 full scans, the orbitrap resolution was 15,000 and the AGC was 2×10^5. For MS/MS in the LTQ, the AGC was 1×10^4. The Mascot algorithm (Matrix Science, USA) was used to identify peptide sequences present in a protein sequence database. Database search criteria were as follows: taxonomy, Homo sapiens, Mus musculus; fixed modification, carbamidomethylated at cysteine residues; variable modification, oxidized at methionine residues; maximum allowed missed cleavages, 2; MS tolerance, 10 ppm; MS/MS tolerance, 0.8 Da. Only peptides resulting from trypsin digests were considered. Peptides were filtered with a significance threshold of $P < 0.05$.

Immunoblots and Immunoprecipitation

Cells and tissues were lysed in RIPA buffer (Sigma-Aldrich) supplemented with protease (GenDEPOT, LLC, Katy, TX, USA) and phosphatase (GenDEPOT, LLC) inhibitors. Equal amounts of proteins (30 μg per lane) from whole-cell or tissue lysates were resolved by SDS-PAGE on 8% to 15% gels, and then transferred to polyvinylidene fluoride (PVDF) membranes. After blocking with 5% non-fat dried milk for 1 hour at RT, membranes were incubated at 4°C overnight with the following primary antibodies: anti-LBH (1:1000; Sigma-Aldrich), anti-Vimentin (1:1000; Sigma-Aldrich), and anti-CRYAB (1:1000; Invitrogen). For immunoprecipitation, 10% (50 μg) of lysate was used as positive control (Input), 500 μg of lysate was incubated with the indicated antibody (1–2 μg) for 3–4 hours at 4°C followed by overnight incubation with Protein A/G PLUS-Agarose (Santa Cruz Biotechnology). Immunoprecipitates were washed five times with RIPA buffer, and then were resolved by SDS–PAGE and immunoblotted with the indicated antibodies. Densitometric analyses of

Western blot bands were performed using Image J software (National Institutes of Health [NIH] 1.34, http://rsbweb.nih.gov/ij/).

Statistical analysis

Results are expressed as the means ± SEMs of at least four independent experiments. The unpaired t test was used to compare two groups, and One-way ANOVA followed by Tukey's post hoc test for four-group comparisons. The analysis was conducted using GraphPad Prism version 8 (GraphPad Software, Inc., La Jolla, CA, USA, www.graphpad.com), and statistical significance was accepted for P values <0.05.

Data availability

The raw data was deposited in Korean Nucleotide Archive (KoNA, https://kobic.re.kr/kona) with the accession ID, PRJKA230548. All data associated with this study are available in the main text or the supplementary materials.

Acknowledgements

This work was funded by the National Research Foundation of Korea (NRF) grants (Guo Nan Yin, NRF-2021R1A2C4002133, Ji-Kan Ryu, 2022R1A2B5B02001671, Jihwan Park, 2019R1C1C1005403 and 2021M3H9A2097520), and a Medical Research Center grant (Ji-Kan Ryu, NRF-2021R1A5A2031612) funded by the Korean government. This work was also supported by the 2023 GIST-MIT Research Collaboration grant funded by the GIST.

References

Abdelbaky T. M., Brock G. B. & Huynh H. (1998). **Improvement of erectile function in diabetic rats by insulin: possible role of the insulin-like growth factor system**. *Endocrinology,* **139,** 3143-3147.

Abdul Y., Jamil S., Li W. & Ergul A. (2023). **Cerebral microvascular matrix metalloproteinase-3 (MMP3) contributes to vascular injury after stroke in female diabetic rats**. *Neurochemistry International,* **162,** 105462.

Angulo J., González-Corrochano R., Cuevas P., Fernández A., Fuente J. M. L., Rolo F., et al. (2010). **Diabetes exacerbates the functional deficiency of NO/cGMP pathway associated with erectile dysfunction in human corpus cavernosum and penile arteries**. *The journal of sexual medicine,* **7,** 758-768.

Anita L., Yin G. N., Hong S.-S., Kang J.-H., Gho Y. S., Suh J.-K., et al. (2022). **Pericyte-derived extracellular vesicle-mimetic nanovesicles ameliorate erectile dysfunction via lipocalin 2 in diabetic mice**. *International Journal of Biological Sciences,* **18,** 3653.

Avolio E. & Madeddu P. (2016). **Discovering cardiac pericyte biology: from physiopathological mechanisms to potential therapeutic applications in ischemic heart disease**. *Vascular pharmacology,* **86,** 53-63.

Ayta I., McKinlay J. & Krane R. (1999). **The likely worldwide increase in erectile dysfunction between 1995 and 2025 and some possible policy consequences**. *BJU international,* **84,** 50-56.

Baek S.-H., Maiorino E., Kim H., Glass K., Raby B. A. & Yuan K. (2022). **Single cell transcriptomic analysis reveals organ specific pericyte markers and identities**. *Frontiers in Cardiovascular Medicine,* **9**.

Bennett N. E., Kim J. H., Wolfe D. P., Sasaki K., Yoshimura N., Goins W. F., et al. (2005). **Improvement in erectile dysfunction after neurotrophic factor gene therapy in diabetic rats**. *The Journal of urology,* **173,** 1820-1824.

Bergers G. & Song S. (2005). **The role of pericytes in blood-vessel formation and maintenance**. *Neuro-oncology,* **7,** 452-464.

Birbrair A., Zhang T., Wang Z.-M., Messi M. L., Mintz A. & Delbono O. (2015). **Pericytes at the intersection between tissue regeneration and pathology**. *Clinical science,* **128,** 81-93.

Bivalacqua T. J., Usta M. F., Champion H. C., Kadowitz P. J. & Hellstrom W. J. (2003). **Endothelial dysfunction in erectile dysfunction: role of the endothelium in erectile physiology and disease**. *Journal of Andrology,* **24,** S17-S37.

Briegel K. J. & Joyner A. L. (2001). **Identification and characterization of Lbh, a novel conserved nuclear protein expressed during early limb and heart development**. *Developmental biology,* **233,** 291-304.

Brown L. S., Foster C. G., Courtney J.-M., King N. E., Howells D. W. & Sutherland B. A. (2019). **Pericytes and neurovascular function in the healthy and diseased brain**. *Frontiers in cellular neuroscience,* **13,** 282.

Browne S., Jha A. K., Ameri K., Marcus S. G., Yeghiazarians Y. & Healy K. E. (2018). **TGF-β1/CD105 signaling controls vascular network formation within growth factor sequestering hyaluronic acid hydrogels**. *PLoS One,* **13,** e0194679.

Burchardt M., Burchardt T., Anastasiadis A. G., Buttyan R., de la Taille A., Shabsigh A., et al. (2005). **Application of angiogenic factors for therapy of erectile dysfunction: protein and DNA transfer of VEGF 165 into the rat penis**. *Urology,* **66,** 665-670.

Cella G., Scattolo N., Vio C., Stevanato F., Lavagnini T., Padovan D., et al. (1986). **Platelet factor 4 (PF4) and heparin released platelet factor 4 (HR-PF4) in diabetes mellitus. Effect of the duration of the disease**. *Folia Haematologica (Leipzig, Germany: 1928),* **113,** 646-654.

Chasseigneaux S., Moraca Y., Cochois-Guégan V., Boulay A.-C., Gilbert A., Le Crom S., et al. (2018). **Isolation and differential transcriptome of vascular smooth muscle cells and mid-capillary pericytes from the rat brain**. *Scientific reports,* **8,** 12272.

Chen K.-Z., Liu S.-X., Li Y.-W., He T., Zhao J., Wang T., et al. (2023). **Vimentin as a potential target for diverse nervous system diseases**. *Neural Regeneration Research,* **18,** 969-975.

Chen Z., Fang Z. & Ma J. (2021). **Regulatory mechanisms and clinical significance of vimentin in breast cancer**. *Biomedicine & Pharmacotherapy,* **133,** 111068.

Dai J., Peng L., Fan K., Wang H., Wei R., Ji G., et al. (2009). **Osteopontin induces angiogenesis through activation of PI3K/AKT and ERK1/2 in endothelial cells**. *Oncogene,* **28,** 3412-3422.

Danielsson F., Peterson M. K., Caldeira Araújo H., Lautenschläger F. & Gad A. K. B. (2018). **Vimentin diversity in health and disease**. *Cells,* **7,** 147.

Dave J. M. & Bayless K. J. (2014). **Vimentin as an integral regulator of cell adhesion and endothelial sprouting**. *Microcirculation,* **21,** 333-344.

De Leonardis F., Colalillo G., Finazzi Agrò E., Miano R., Fuschi A. & Asimakopoulos A. D. (2022).

Endothelial dysfunction, erectile deficit and cardiovascular disease: an overview of the pathogenetic links. *Biomedicines,* **10,** 1848.

Desai A., Chen R., Cayetano A., Jayasena C. N. & Minhas S. (2023). **Understanding and treating ejaculatory dysfunction in men with diabetes mellitus**. *Andrology,* **11,** 379-398.

Dimberg A., Rylova S., Dieterich L. C., Olsson A.-K., Schiller P., Wikner C., et al. (2008). **αB-crystallin promotes tumor angiogenesis by increasing vascular survival during tube morphogenesis**. *Blood, The Journal of the American Society of Hematology,* **111,** 2015-2023.

Ferland-McCollough D., Slater S., Richard J., Reni C. & Mangialardi G. (2017). **Pericytes, an overlooked player in vascular pathobiology**. *Pharmacology & therapeutics,* **171,** 30-42.

Gerhardt H. & Betsholtz C. (2003). **Endothelial-pericyte interactions in angiogenesis**. *Cell and tissue research,* **314,** 15-23.

Ghatak K., Yin G. N., Hong S.-S., Kang J.-H., Suh J.-K. & Ryu J.-K. (2022). **Heat Shock Protein 70 in Penile Neurovascular Regeneration Requires Cystathionine Gamma-Lyase**. *The World Journal of Men's Health,* **40,** 580.

Gonzales A. L., Klug N. R., Moshkforoush A., Lee J. C., Lee F. K., Shui B., et al. (2020). **Contractile pericytes determine the direction of blood flow at capillary junctions**. *Proceedings of the National Academy of Sciences,* **117,** 27022-27033.

Guo M., Ehrlicher A. J., Mahammad S., Fabich H., Jensen M. H., Moore J. R., et al. (2013). **The role of vimentin intermediate filaments in cortical and cytoplasmic mechanics**. *Biophysical journal,* **105,** 1562-1568.

Guo M., Zhang H., Zheng J. & Liu Y. (2020). **Glypican-3: a new target for diagnosis and treatment of hepatocellular carcinoma**. *Journal of Cancer,* **11,** 2008.

Haghighi K., Bidwell P. & Kranias E. G. (2014). **Phospholamban interactome in cardiac contractility and survival: A new vision of an old friend**. *Journal of molecular and cellular cardiology,* **77,** 160-167.

Hu L., Qi S., Zhang K. & Fu Q. (2018). **Essential role of brain□derived neurotrophic factor (bdnf) in diabetic erectile dysfunction**. *Andrologia,* **50,** e12924.

Ismail E., Younis S., Ismail I., El□Wazir Y. & El□Sakka A. (2020). **Early administration of phosphodiesterase 5 inhibitors after induction of diabetes in a rat model may prevent erectile dysfunction**. *Andrology,* **8,** 241-248.

Jiang Y., Zhou J., Zou D., Hou D., Zhang H., Zhao J., et al. (2019). **Overexpression of Limb-Bud and Heart (LBH) promotes angiogenesis in human glioma via VEGFA-mediated ERK signalling under hypoxia**. *EBioMedicine,* **48,** 36-48.

Jin H.-R., Kim W. J., Song J. S., Piao S., Choi M. J., Tumurbaatar M., et al. (2011). **Intracavernous delivery of a designed angiopoietin-1 variant rescues erectile function by enhancing endothelial regeneration in the streptozotocin-induced diabetic mouse**. *Diabetes,* **60,** 969-980.

Jin H. R., Kim W. J., Song J. S., Choi M. J., Piao S., Shin S. H., et al. (2009). **Functional and morphologic characterizations of the diabetic mouse corpus cavernosum: Comparison of a multiple low□dose and a single high□dose streptozotocin protocols**. *The Journal of Sexual Medicine,* **6,** 3289-3304.

Kessler A., Sollie S., Challacombe B., Briggs K. & Van Hemelrijck M. (2019). **The global prevalence of erectile dysfunction: a review**. *BJU international,* **124,** 587-599.

Kowalczyk A., Kleniewska P., Kolodziejczyk M., Skibska B. & Goraca A. (2015). **The role of endothelin-1 and endothelin receptor antagonists in inflammatory response and sepsis**. *Archivum immunologiae et therapiae experimentalis,* **63,** 41-52.

Kubin M., Wagner G. & Fugl-Meyer A. R. (2003). **Epidemiology of erectile dysfunction**. *International journal of impotence research,* **15,** 63-71.

Kumar A., D'Souza S. S., Moskvin O. V., Toh H., Wang B., Zhang J., et al. (2017). **Specification and diversification of pericytes and smooth muscle cells from mesenchymoangioblasts**. *Cell reports,* **19,** 1902-1916.

Kyriakides T. R., Hartzel T., Huynh G. & Bornstein P. (2001). **Regulation of angiogenesis and matrix remodeling by localized, matrix-mediated antisense gene delivery**. *Molecular Therapy,* **3,** 842-849.

Lee M. J., Na K., Jeong S.-K., Lim J.-S., Kim S. A., Lee M.-J., et al. (2014). **Identification of human complement factor B as a novel biomarker candidate for pancreatic ductal adenocarcinoma**. *Journal of proteome research,* **13,** 4878-4888.

Leung A. C., Christ G. J. & Melman A. (2004). **Physiology of penile erection and pathophysiology of erectile dysfunction**. *Atlas of Male Sexual Dysfunction***,** 1-25.

Li T., Forbes M. E., Fuller G. N., Li J., Yang X. & Zhang W. (2020). **IGFBP2: integrative hub of developmental and oncogenic signaling network**. *Oncogene,* **39,** 2243-2257.

Lin C. G., Leu S.-J., Chen N., Tebeau C. M., Lin S.-X., Yeung C.-Y., et al. (2003). **CCN3 (NOV) is a novel**

angiogenic regulator of the CCN protein family. *Journal of Biological Chemistry,* **278,** 24200-24208.
Liu C.-Y., Lin H.-H., Tang M.-J. & Wang Y.-K. (2015). **Vimentin contributes to epithelial-mesenchymal transition cancer cell mechanics by mediating cytoskeletal organization and focal adhesion maturation**. *Oncotarget,* **6,** 15966.
Liu Q., Song Y., Cui Y., Hu C., Luo Y., Hu D., et al. (2023). **Heterogeneity of fibroblasts is a hallmark of age-associated erectile dysfunction**. *The International Journal of Biochemistry & Cell Biology,* **156,** 106343.
Liu Y., Zhang H., Wang S., Guo Y., Fang X., Zheng B., et al. (2021). **Reduced pericyte and tight junction coverage in old diabetic rats are associated with hyperglycemia-induced cerebrovascular pericyte dysfunction**. *American Journal of Physiology-Heart and Circulatory Physiology,* **320,** H549-H562.
Luo H., Xia X., Kim G. D., Liu Y., Xue Z., Zhang L., et al. (2021). **Characterizing dedifferentiation of thyroid cancer by integrated analysis**. *Science Advances,* **7,** eabf3657.
Miner M. M. (2011). **Erectile dysfunction: a harbinger or consequence: does its detection lead to a window of curability?** *Journal of andrology,* **32,** 125-134.
Moisan E., Chiasson S. & Girard D. (2007). **The intriguing normal acute inflammatory response in mice lacking vimentin**. *Clinical & Experimental Immunology,* **150,** 158-168.
Neng L., Zhang W., Hassan A., Zemla M., Kachelmeier A., Fridberger A., et al. (2013). **Isolation and culture of endothelial cells, pericytes and perivascular resident macrophage-like melanocytes from the young mouse ear**. *nature protocols,* **8,** 709-720.
Neubauer-Geryk J., Kozera G. M., Wolnik B., Szczyrba S., Nyka W. M. & Bieniaszewski L. (2012). **Angiogenin in middle-aged type 1 diabetes patients**. *Microvascular Research,* **84,** 387-389.
Park J., Shrestha R., Qiu C., Kondo A., Huang S., Werth M., et al. (2018). **Single-cell transcriptomics of the mouse kidney reveals potential cellular targets of kidney disease**. *Science,* **360,** 758-763.
Pourhaghighi R., Ash P. E., Phanse S., Goebels F., Hu L. Z., Chen S., et al. (2020). **BraInMap elucidates the macromolecular connectivity landscape of mammalian brain**. *Cell systems,* **10,** 333-350. e14.
Powder K. E., Cousin H., McLinden G. P. & Craig Albertson R. (2014). **A nonsynonymous mutation in the transcriptional regulator lbh is associated with cichlid craniofacial adaptation and neural crest cell development**. *Molecular biology and evolution,* **31,** 3113-3124.
Reddy M. A., Das S., Zhuo C., Jin W., Wang M., Lanting L., et al. (2016). **Regulation of vascular smooth muscle cell dysfunction under diabetic conditions by miR-504**. *Arteriosclerosis, thrombosis, and vascular biology,* **36,** 864-873.
Rieger M. E., Sims A. H., Coats E. R., Clarke R. B. & Briegel K. J. (2010). **The embryonic transcription cofactor LBH is a direct target of the Wnt signaling pathway in epithelial development and in aggressive basal subtype breast cancers**. *Molecular and cellular biology,* **30,** 4267-4279.
Sáenz de Tejada I. i., Anglin G., Knight J. R. & Emmick J. T. (2002). **Effects of tadalafil on erectile dysfunction in men with diabetes**. *Diabetes care,* **25,** 2159-2164.
Shannon P., Markiel A., Ozier O., Baliga N. S., Wang J. T., Ramage D., et al. (2003). **Cytoscape: a software environment for integrated models of biomolecular interaction networks**. *Genome research,* **13,** 2498-2504.
Shimizu F., Sano Y., Haruki H. & Kanda T. (2011). **Advanced glycation end-products induce basement membrane hypertrophy in endoneurial microvessels and disrupt the blood–nerve barrier by stimulating the release of TGF-β and vascular endothelial growth factor (VEGF) by pericytes**. *Diabetologia,* **54,** 1517-1526.
Smyth L. C., Rustenhoven J., Scotter E. L., Schweder P., Faull R. L., Park T. I., et al. (2018). **Markers for human brain pericytes and smooth muscle cells**. *Journal of chemical neuroanatomy,* **92,** 48-60.
Souza I. L. L. d., Ferreira E. d. S., Vasconcelos L. H. C., Cavalcante F. d. A. & Silva B. A. d. (2022). **Erectile dysfunction: key role of cavernous smooth muscle cells**. *Frontiers in Pharmacology,* **13,** 895044.
Sullivan C. J., Teal T. H., Luttrell I. P., Tran K. B., Peters M. A. & Wessells H. (2005). **Microarray analysis reveals novel gene expression changes associated with erectile dysfunction in diabetic rats**. *Physiological genomics.*
Sun Y., Hu X., Zhang K., Rao M., Yin P. & Dong R. (2022). **A Single-Cell Survey of Cellular Heterogeneity in Human Great Saphenous Veins**. *Cells,* **11,** 2711.
Thorve V. S., Kshirsagar A. D., Vyawahare N. S., Joshi V. S., Ingale K. G. & Mohite R. J. (2011). **Diabetes-induced erectile dysfunction: epidemiology, pathophysiology and management**. *Journal of diabetes and its complications,* **25,** 129-136.
Warmke N., Griffin K. J. & Cubbon R. M. (2016). **Pericytes in diabetes-associated vascular disease**. *Journal of Diabetes and its Complications,* **30,** 1643-1650.
Wei A., He S., Zhao J., Liu Y., Hu Y., Zhang T., et al. (2012). **Characterization of corpus cavernosum smooth**

muscle cell phenotype in diabetic rats with erectile dysfunction. *International journal of impotence research,* **24,** 196-201.

Winkler E. A., Sagare A. P. & Zlokovic B. V. (2014). **The Pericyte: A Forgotten Cell Type with Important Implications for A lzheimer's Disease?** *Brain pathology,* **24,** 371-386.

Wittrisch S., Klöting N., Mörl K., Chakaroun R., Blüher M. & Beck-Sickinger A. G. (2020). **NPY1R-targeted peptide-mediated delivery of a dual PPARα/γ agonist to adipocytes enhances adipogenesis and prevents diabetes progression**. *Molecular Metabolism,* **31,** 163-180.

Wu A., Luo N., Xu Y., Du N., Li L. & Liu Q. (2022). **Exosomal LBH inhibits epithelial-mesenchymal transition and angiogenesis in nasopharyngeal carcinoma via downregulating VEGFA signaling**. *International Journal of Biological Sciences,* **18,** 242.

Wu A., Zhang L., Luo N., Zhang L., Li L. & Liu Q. (2021). **Limb-bud and heart (LBH) inhibits cellular migration, invasion and epithelial-mesenchymal transition in nasopharyngeal carcinoma via downregulating αB-crystallin expression**. *Cellular Signalling,* **85,** 110045.

Yin G. N. (2022). **Pericyte-derived heme-binding protein 1 promotes angiogenesis and improves erectile function in diabetic mice**. *Investigative and Clinical Urology,* **63,** 464.

Yin G. N., Das N. D., Choi M. J., Song K.-M., Kwon M.-H., Ock J., et al. (2015). **The pericyte as a cellular regulator of penile erection and a novel therapeutic target for erectile dysfunction**. *Scientific Reports,* **5,** 10891.

Yin G. N., Jin H.-R., Choi M.-J., Limanjaya A., Ghatak K., Minh N. N., et al. (2018). **Pericyte-derived Dickkopf2 regenerates damaged penile neurovasculature through an angiopoietin-1-Tie2 pathway**. *Diabetes,* **67,** 1149-1161.

Yin G. N., Kim D.-K., Kang J. I., Im Y., Lee D. S., Han A.-r., et al. (2022). **Latrophilin-2 is a novel receptor of LRG1 that rescues vascular and neurological abnormalities and restores diabetic erectile function**. *Experimental & Molecular Medicine,* **54,** 626-638.

Yin G. N., Ock J., Choi M. J., Song K. M., Ghatak K., Minh N. N., et al. (2020). **A Simple and Nonenzymatic Method to Isolate Human Corpus Cavernosum Endothelial Cells and Pericytes for the Study of Erectile Dysfunction**. *World J Mens Health,* **38,** 123-131. 10.5534/wjmh.180091.

Yin G. N., Wu J., Cui Y., Lin C., Shi L., Gao Z.-L., et al. (2021). **Transcriptional profiling of mouse cavernous pericytes under high-glucose conditions: Implications for diabetic angiopathy**. *Investigative and Clinical Urology,* **62,** 100.

Zacchigna S., Lambrechts D. & Carmeliet P. (2008). **Neurovascular signalling defects in neurodegeneration**. *Nature Reviews Neuroscience,* **9,** 169-181.

Zhao L., Han S., Su H., Li J., Zhi E., Li P., et al. (2022). **Single-cell transcriptome atlas of the human corpus cavernosum**. *Nature communications,* **13,** 4302.

Figure Legends

Fig. 1. Single cell transcriptional landscape of mouse cavernous tissues in normal and diabetic conditions. (**A**) Schematic workflow of this study. Cavernous tissues from sixteen-week-old male mice were used for single cell RNA sequencing (n=5 for each group). DM, diabetes mellitus. (**B**) Visualization of single cell data from mouse cavernous tissues using UMAP. Each cell type is indicated by a different color. FCP, fibrochondrocyte progenitors; FC, fibrochondrocytes; Chond, chondrocytes; FB, fibroblasts; Myo-FB, myofibroblasts; LEC, lymphatic endothelial cells; VEC, vascular endothelial cells; SMC, smooth muscle cells. (**C**) Heatmap of known cell type marker genes used for annotation. (**D**) UMAP projection of four fibroblast clusters and expression of marker genes of four fibroblast subsets. *Egr1* for *Egr1* high FB; *Cxcl12* for *Cxcl12* high FB; *Mgp* for Reticular FB; *Rps25* and *Rps17* for Ribosomal gene high FB. (**E**) Dot plot showing the expression of top five marker genes of each fibroblast subset. (**F**) DEGs between diabetic and normal conditions in Fibroblasts. The top 10 (based on log-fold change) DEGs are indicated with gene names, and genes identified as having high or low expression in diabetes in previous studies are indicated with gene names in red or blue. DEGs with adjusted p-value > 0.05 were indicated in gray. (**G**) Gene ontology analysis of the DEGs higher in normal compared to diabetes in Fibroblasts. (**H**) Gene ontology analysis of the DEGs higher in diabetes compared to normal in Fibroblasts.

Fig. 2. Identification of *Lbh* as a marker of pericytes. (**A**) Expression of well-known marker genes of SMC and Pericyte (*Cnn1* for SMC, *Rgs5* and *Pdgfrb* for Pericyte). (**B**) Significantly enriched gene sets associated with function of SMC and Pericyte. Gene sets with positive normalized enrichment score (NES) are enriched in Pericyte, and negative values are enriched in SMC. (**C**) Violin plots showing expression of *Lbh* in each cell type. (**D** and **E**) LBH (red)/a-SMA (green) and LBH (red)/CD31(green) staining in MCPs, aorta SMC, and bladder tissues. Nuclei were labeled with DAPI (blue). Scale bars, 25 µm (MCPs and aorta SMC), 50 µm (bladder top panel) and 100 µm (bladder bottom panel). (**F** and **G**) CD31 (blue)/a-SMA (green)/LBH (red) and LBH (red)/PDGFRβ (green) staining in mouse dorsal vein and dorsal artery tissues. Nuclei were labeled with DAPI (bottom panel, blue). Scale bars, 25 µm (dorsal artery) and 50 µm (dorsal vein). Arrows indicate the LBH expressed pericytes. MCPs, mouse cavernous pericytes; SMC, smooth muscle cell; DAPI, 4,6-diamidino-2-phenylindole. ***$P < 0.001$ by DESeq2 test.

Fig. 3. Cell-cell interactions between pericytes and other cell types in normal and diabetes. (**A**) CellphoneDB dot plots showing angiogenesis-associated ligand-receptor interactions from pericytes to other cell types in normal and diabetic samples. P-values are indicated as circle sizes. The means of the average expression level of the interaction are indicated by color. (**B**) CellphoneDB dot plots showing angiogenesis-associated ligand-receptor interactions from other cell types to pericytes in normal and diabetic samples. P-values are indicated as circle sizes. The means of the average expression level of the interaction are indicated by color. (**C**) The inferred VEGF signaling pathway network in normal and diabetes using CellChat. The width of line represents the communication probability. The color of line matches the sender of the signal. (**D**) GSEA plots showing the gene sets downregulated in diabetic pericytes compared to normal pericytes. (**E**) Heatmap showing the regulon activities of angiogenesis-related transcription factors in pericytes and SMCs in normal and diabetes. Scaled values of regulon activity scores are displayed on the heatmap. $^{**}P < 0.01$; $^{***}P < 0.001$ by generalized linear model. (**F**) Proteome profiler mouse angiogenesis array analysis of mouse penis tissues from age-matched control and diabetic mice. The relative expression of each protein was determined by comparing the respective plots to the positive control (reference spot). The frame dot line indicates changed proteins between control and diabetic mice. Expression of the indicated proteins was quantified by assessing the intensity of the dot using Image J. DM, diabetes mellitus.

Fig. 4. LBH improves erectile function under diabetic conditions through induction of neurovascular regeneration. (**A** and **B**) Representative images of immunofluorescence staining of LBH (green)/CD140b (red) in cavernosum tissues and LBH (red) in MCPs under normal and diabetic conditions (*in vivo* and *in vitro*). Nuclei were labeled with DAPI (blue). Scale bar, 100 µm. (**C** and **D**) Quantification of LBH or CD140b expression in *in vivo* and *in vitro* by using Image J, and results are presented as means ± SEM (n = 4). (**E**) Representative western blots for LBH of MCPs under NG and HG conditions, and mouse penis tissues from age-matched control and diabetic mice. (**F**) Normalized band intensity ratio of LBH to β-actin was quantified using Image J, and results are presented as means ± SEM (n = 4). (**G**) Representative intracavernous pressure (ICP) responses for the age-matched control and diabetic mice stimulated at 2 weeks after intracavernous injections with PBS, lentiviruses ORF control particles (NC), and ORF clone of mouse *Lbh* (LBH O/E) (20 µL for PBS, 5 $x10^4$ IFU/mouse for lentiviral particles). The stimulus interval is indicated by a solid bar. (**H**) Ratios of mean maximal ICP and total ICP (area under the curve) versus MSBP were calculated for each group, and the results are presented as means ± SEM (n = 5). (**I** and **J**) Cavernous CD31 (endothelial cell, red), NG2 (pericyte, green), neurofilament (red), and nNOS (green) staining in cavernous tissues from age-matched control (C) and diabetic mice stimulated at 2 weeks after intracavernous injections with lentiviruses ORF control particles (NC) and ORF clone of mouse *Lbh* (LBH O/E). Scale bars, 100 µm (left), 25 µm (right). (**K-N**) Quantitative analysis of cavernous endothelial cell, pericyte, and neuronal cell content were quantified by Image J, and results are presented as means ± SEM (n = 4). The relative ratio in the NG or control group was defined as 1. **P < 0.01; ***P < 0.001. DM, diabetes mellitus; PBS, phosphate-buffered saline; MCPs, mouse cavernous pericytes; NG, normal glucose; HG, high glucose; DAPI, 4,6-diamidino-2-phenylindole; MSBP, mean systolic blood pressure; ns, not significant.

Fig. 5. LBH as a marker of pericyte in human corpus cavernosum. (**A**) Visualization of single cell data from human corpus cavernosum using UMAP. Each cell type is indicated by a different color. EC, endothelial cells; FB, Fibroblasts; SMC, Smooth muscle cell; MFB, Myofibroblast; SWC, Schwann cell; MAC, Macrophage; T, T cell. (**B**) Expression of marker genes of SMC (*ACTA2* and *CNN1*) and marker genes of Pericyte (*RGS5* and *LBH*). (**C**) Biological processes identified through gene ontology analysis of clusters annotated as Pericyte, SMC, and MFB. (**D**) LBH (green) staining in cavernous tissues from two patients with diabetic erectile dysfunction and two patients with congenital penile curvature who had normal erectile function during reconstructive penile surgery. Scale bar, 100 µm. (**E**) LBH (red) staining in primary cultured human cavernous pericytes under NG and HG conditions for 3 days. (**F** and **G**) LBH immunopositive areas were quantified by Image J, and results are presented as means ± SEM (n = 4). Nuclei were labeled with DAPI (blue). The relative ratio in the control or NG group was defined as 1. ***P < 0.001. NG, normal glucose; HG, high glucose; DM, diabetes mellitus; DAPI, 4,6-diamidino-2-phenylindole.

Fig. 6. LBH-interacting protein identification in mouse cavernous pericytes. (**A**) LBH was immunoprecipitated (IP) from whole-MCPs lysates, resolved on SDS-PAGE gels, and stained with Coomassie blue solution. Gel bands indicated by red frame dot line were analyzed by liquid chromatography tandem mass spectrometry (LC-MS/MS) analysis. (**B**) Co-IP of LBH, CRYAB and Vimentin from whole-MCPs lysates followed by immunoblot analysis to detect CRYAB, Vimentin and LBH. (**C** and **D**) Representative images of immunofluorescence staining of LBH (green)/CRYAB (red) and LBH (green)/VIM (red) in normal penis tissues and MCPs. Nuclei were labeled with DAPI (blue). Scale bar, 100 μm (top), 25 μm (bottom). (**E**) Protein-protein interaction network of LBH, CRYAB, VIM, and 1st and 2nd interactors of LBH. Lines connecting molecules show interaction sources in color. (**F**) Biological pathways involving molecules in PPI network identified by gene ontology analysis. (**G**) Significantly enriched gene sets associated with angiogenesis and nerve system in normal pericytes compared to diabetic pericytes in single cell data. (**H**) Representative western blots for CRYAB and VIM of MCPs under NG and HG conditions (left), and mouse penis tissues from age-matched control and diabetic mice (right). (**I**) Normalized band intensity ratio of CRYAB and VIM to β-actin was quantified using Image J, and results are presented as means ± SEM (n = 4). The relative ratio in the NG or control group was defined as 1. **P < 0.01; ***P < 0.001. MCPs, mouse cavernous pericytes; NG, normal glucose; HG, high glucose; DM, diabetes mellitus; DAPI, 4,6-diamidino-2-phenylindole.

Supplementary Information

Fig. S1. Chondrocyte subsets in single cell RNA sequencing data of mouse cavernous tissues. (**A**) UMAP projection of three chondrocyte clusters in single cell data of mouse cavernous tissues. (**B**) Expression of marker genes of three chondrocyte subsets. *Mylk* and *Col3a1* for FCP; *Prg4* and *Anxa8* for differentiating FC; *Spink5* for *Spink5*+ Chond. (**C**) Dot plot showing the expression of top five marker genes of each chondrocyte subset. The color represents the average expression level, and the size of the dots represents the percentage of cells expressing each gene.

Fig. S2. Volcano plots showing DEGs between diabetic and normal conditions in each cell type. (**A**) DEGs between diabetic and normal conditions in Chondrocytes. (**B**) DEGs between diabetic and normal conditions in Myo-FB. (**C**) DEGs between diabetic and normal conditions in Valve-related LEC. (**D**) DEGs between diabetic

and normal conditions in VEC. (**E**) DEGs between diabetic and normal conditions in SMC. (**F**) DEGs between diabetic and normal conditions in Pericyte. (**G**) DEGs between diabetic and normal conditions in Macrophage. The top 10 (based on log-fold change) DEGs are indicated with gene names, and genes identified as having high or low expression in diabetes in previous studies are indicated with gene names in red or blue. DEGs with adjusted p-value > 0.05 were indicated in gray. The LEC was not shown as a volcano plot because there were only two significant DEGs, and Schwann cells have no significant DEG (adjusted p-value < 0.05).

Fig. S3. Gene ontology high in normal compared to diabetes in each cell type. (**A**) Gene ontology analysis of the genes higher in normal compared to diabetes in Chondrocytes. (**B**) Gene ontology analysis of the genes higher in normal compared to diabetes in Myo-FB. (**C**) Gene ontology analysis of the genes higher in normal compared to diabetes in Valve-related LEC. (**D**) Gene ontology analysis of the genes higher in normal compared to diabetes in Pericyte. (**E**) Gene ontology analysis of the genes higher in normal compared to diabetes in Macrophage. There was no significant term in LEC, VEC, SMC, and Schwann cells (p-value < 0.05 and FDR < 0.25).

Fig. S4. Gene ontology high in diabetes compared to normal in each cell type. (**A**) Gene ontology analysis of the genes higher in diabetes compared to normal in Chondrocytes. (**B**) Gene ontology analysis of the genes higher in diabetes compared to normal in Myo-FB. (**C**) Gene ontology analysis of the genes higher in diabetes compared to normal in Valve-related LEC. (**D**) Gene ontology analysis of the genes higher in diabetes compared to normal in Pericyte. (**E**) Gene ontology analysis of the genes higher in diabetes compared to normal in Macrophage. There were no significant terms in LEC and Schwann cells (P-value < 0.05 and FDR < 0.25), and only translation-related terms were identified in VEC and SMC.

Fig. S5. Pericyte-specifically expressed genes in single-cell RNA sequencing data. (A) Violin plots showing the expression of known marker genes of pericyte (*Cspg4, Kcnj8, Higd1b, Cox4i2*) and SMC (*Acta2, Myh11, Tagln, Actg2*). **(B)** Violin plots showing the expression of *Ednra, Gpc3, Npy1r, Pln,* and *Atp1b2* in each cell type of mouse cavernous tissues. **(C)** AUC scores of *Rgs5, Lbh, Endra, Gpc3, Npylr, Pln*, and *Atplb2*. **(D)** ATP1B2 (red)/a-SMA (green) staining in MCPs and aorta SMC. Scale bars, 25 µm. **(E)** LBH (red)/a-SMA (green) and LBH (red)/CD31(green) staining in MCPs, aorta SMC. Scale bars, 100 µm. The nuclei were stained with DAPI (blue). Percentage of relative markers expressed cells. MCPs, mouse cavernous pericytes; SMC, smooth muscle cells.

Fig. S6. Expressions of *Lbh* in single-cell RNA sequencing data from tissues other than the penis. ALH, Ascending limb of loop of Henle; PST, Proximal straight tubule. (**A-D**) Violin plots showing the expression of endothleial cell marker (*Pecam1*), known pericyte markers (*Rgs5, Pdgfrb, Cspg4*) and *Lbh* in mouse bladder (A), heart and aorta (**B**), kidney (**C**), trachea (**D**) from Tabula Muris.

Fig. S7. Cell-cell interactions between pericytes and other cell types showing significant differences in between normal and diabetes. CellphoneDB dot plots showing ligand-receptor interactions between pericytes and other cell types in normal and diabetes. The plot shows all ligand-receptor interactions with significant differences between diabetes and normal. P-values are indicated as circle sizes. The means of the average expression level of the interaction are indicated by color.

Fig. S8. Cell-cell communication between cell types in normal and diabetes using CellChat. (**A**) The inferred FGF signaling network in normal and diabetes. (**B**) The inferred NT signaling network in normal and diabetes. (**C**) The inferred PDGF signaling network in normal and diabetes. (**D**) The inferred JAM signaling network in normal and diabetes. (**E**) The inferred COLLAGEN signaling network in normal and diabetes. (**F**) The inferred BMP signaling network in normal and diabetes. The width of line represents the communication probability. The color of line matches the sender of the signal.

Fig. S9. RT-PCR validation of differentially expressed genes from single cell RNA sequencing analyses in MCPs exposed to NG or HG conditions for 72 hours. (**A**) Representative RT-PCR for *Lmo2, Junb, Elk1, Hoxd10* in MCPs. (**B-E**) Normalized band intensity values (n=4). *P < 0.05 vs. NG group. The relative ratio of the NG group was arbitrarily set to 1. NG, normal glucose; HG, high glucose.

Fig. S10. LBH immunofluorescence staining in corpus cavernosum tissues after infection with lentiviruses containing ORF mouse clone of *Lbh*. (**A**) immunofluorescence staining of CD31 (green) and LBH (red) in corpus cavernosum tissues treated with lentiviruses ORF control particles (NC) and ORF clone of mouse *Lbh* (LBH O/E) in diabetic mice. Nuclei were labeled with DAPI (blue). Scale bars, 50 μm. (**B**) Quantification of LBH positive area by Image J, and results are presented as means ± SEM (n = 4). The relative ratio in the Control group was defined as 1. *P < 0.05; ***P < 0.001. DM, diabetes mellitus; DAPI, 4,6-diamidino-2-phenylindole.

Fig. S11. LBH enhances pericyte angiogenesis and MPG neurite sprouting under high glucose conditions. (**A, B, C, G**, and **I**) TUNEL assay (**A**, green), immunofluorescence staining of PH3 (**B**, red), migration (**C**), tube formation (**G**) in MCPs, and immunofluorescence staining with neurofilament in MPG tissues (**I**, green) treated with lentiviruses ORF control particles (NC) and ORF clone of mouse *Lbh* (LBH O/E) under HG conditions. Nuclei were labeled with DAPI (blue). Scale bars, 50 μm. (**D, E, F, H**, and **J**) Quantification of number of TUNEL positive cells (arrow indicated, **D**), PH3 positive cells (arrow indicated, **E**), ratio of migrated cells (cells in red frame dot line, **F**), master junctions (**H**), and fold change of MPG sprouting (**J**) by Image J, and results are presented as means ± SEM (n = 4). The relative ratio in the NG group was defined as 1. *P < 0.05; **P < 0.01; ***P < 0.001. TUNEL, terminal deoxynucleotidyl transferase-mediated deoxyuridine triphosphate nick end labeling; NG, normal glucose; HG, high glucose; DM, diabetes mellitus; DAPI, 4,6-diamidino-2-phenylindole; MPG, major pelvic ganglion.

Fig. S12. Expression of marker genes of pericyte and smooth muscle cells in human penis single cell RNA sequencing data. (A) Violin plots showing known pericyte marker genes, *CSPG4* and *COX4I2*. **(B)** A violin plot showing known SMC marker genes, *ACTG2*. EC, endothelial cells;FB, Fibroblasts; SMC, Smooth muscle cells; MFB, Myofibroblast; SWC, Schwann cells; MAC, Macrophage;T, T cell.

Table S1. Relative density of mouse angiogenesis array spots

Table S2. Physiologic and metabolic parameters: 2 weeks after treatment with PBS, NC, LBH O/E

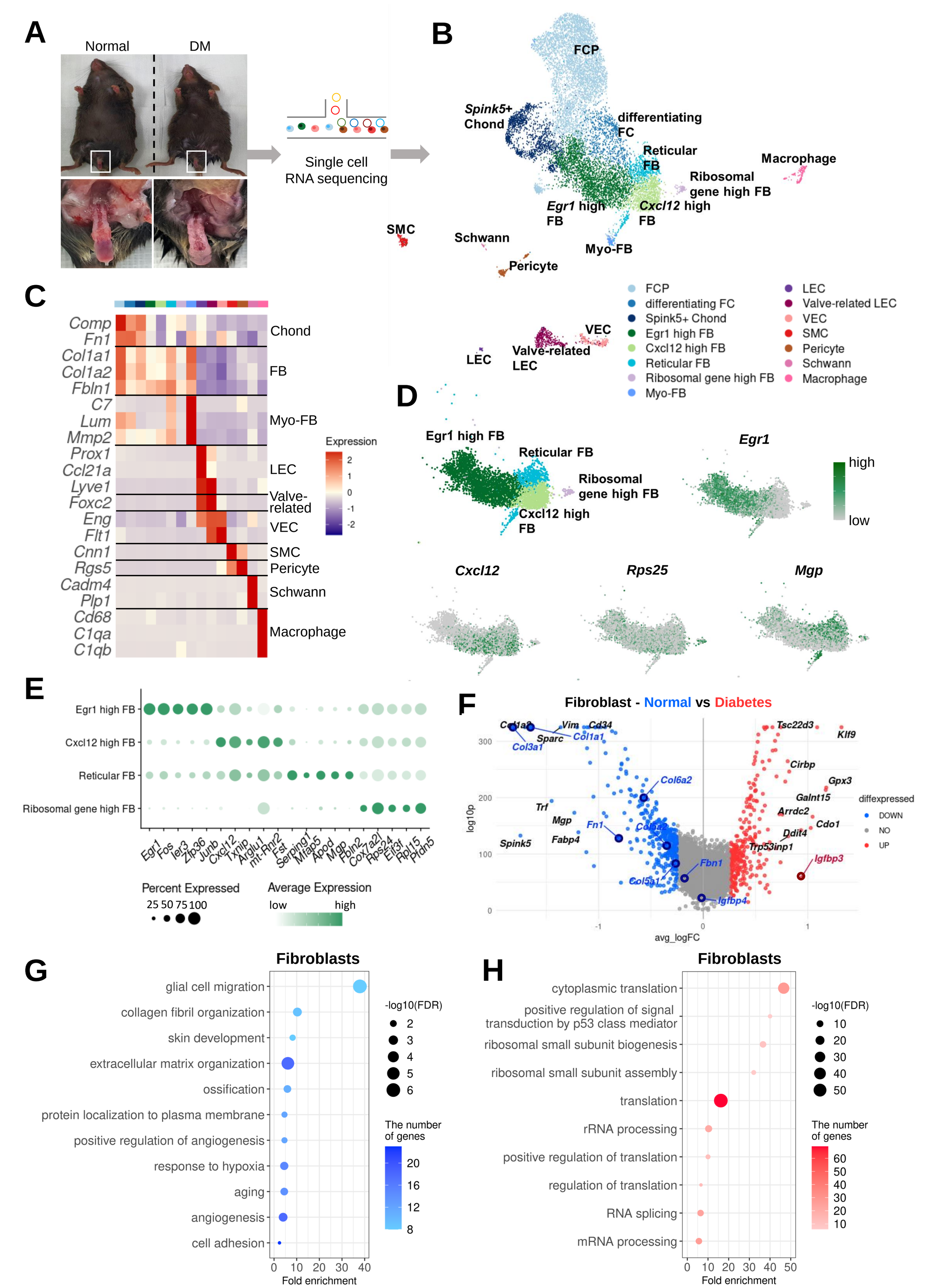
A
Normal
DM
Single cell
RNA sequencing
B
FCP
Spink5+
Chond
differentiating
FC
Reticular
FB
Macrophage
Ribosomal
gene high FB
Egr1 high
FB
Cxcl12 high
FB
SMC
Schwann
Myo-FB
Pericyte
VEC
LEC
Valve-related
LEC
FCP
differentiating FC
Spink5+ Chond
Egr1 high FB
Cxcl12 high FB
Reticular FB
Ribosomal gene high FB
Myo-FB
LEC
Valve-related LEC
VEC
SMC
Pericyte
Schwann
Macrophage
C
Comp
Fn1
Col1a1
Col1a2
Fbln1
C7
Lum
Mmp2
Prox1
Ccl21a
Lyve1
Foxc2
Eng
Flt1
Cnn1
Rgs5
Cadm4
Plp1
Cd68
C1qa
C1qb
Chond
FB
Myo-FB
LEC
Valve-related
VEC
SMC
Pericyte
Schwann
Macrophage
Expression
2
1
0
-1
-2
D
Egr1 high FB
Reticular FB
Ribosomal
gene high FB
Cxcl12 high
FB
Egr1
high
low
Cxcl12
Rps25
Mgp
E
Egr1 high FB
Cxcl12 high FB
Reticular FB
Ribosomal gene high FB
Egr1
Fos
Ier3
Zfp36
Junb
Cxcl12
Txnip
Arglu1
mt-Rnr2
Fst
Serping1
Mfap5
Apod
Mgp
Fbln2
Cox7a2l
Rps24
Eif3f
Rpl15
Pfdn5
Percent Expressed
25 50 75 100
Average Expression
low
high
F
Fibroblast - Normal vs Diabetes
Col1a2
Vim
Cd34
Sparc
Col1a1
Col3a1
Tsc22d3
Klf9
Cirbp
Gpx3
Galnt15
Arrdc2
Cdo1
Ddit4
Trp53inp1
Igfbp3
Col6a2
Trf
Mgp
Fn1
Col1a2
Fabp4
Spink5
Fbn1
Col5a1
Igfbp4
log10p
avg_logFC
diffexpressed
DOWN
NO
UP
G
Fibroblasts
glial cell migration
collagen fibril organization
skin development
extracellular matrix organization
ossification
protein localization to plasma membrane
positive regulation of angiogenesis
response to hypoxia
aging
angiogenesis
cell adhesion
Fold enrichment
-log10(FDR)
2
3
4
5
6
The number
of genes
20
16
12
8
H
Fibroblasts
cytoplasmic translation
positive regulation of signal
transduction by p53 class mediator
ribosomal small subunit biogenesis
ribosomal small subunit assembly
translation
rRNA processing
positive regulation of translation
regulation of translation
RNA splicing
mRNA processing
Fold enrichment
-log10(FDR)
10
20
30
40
50
The number
of genes
60
50
40
30
20
10

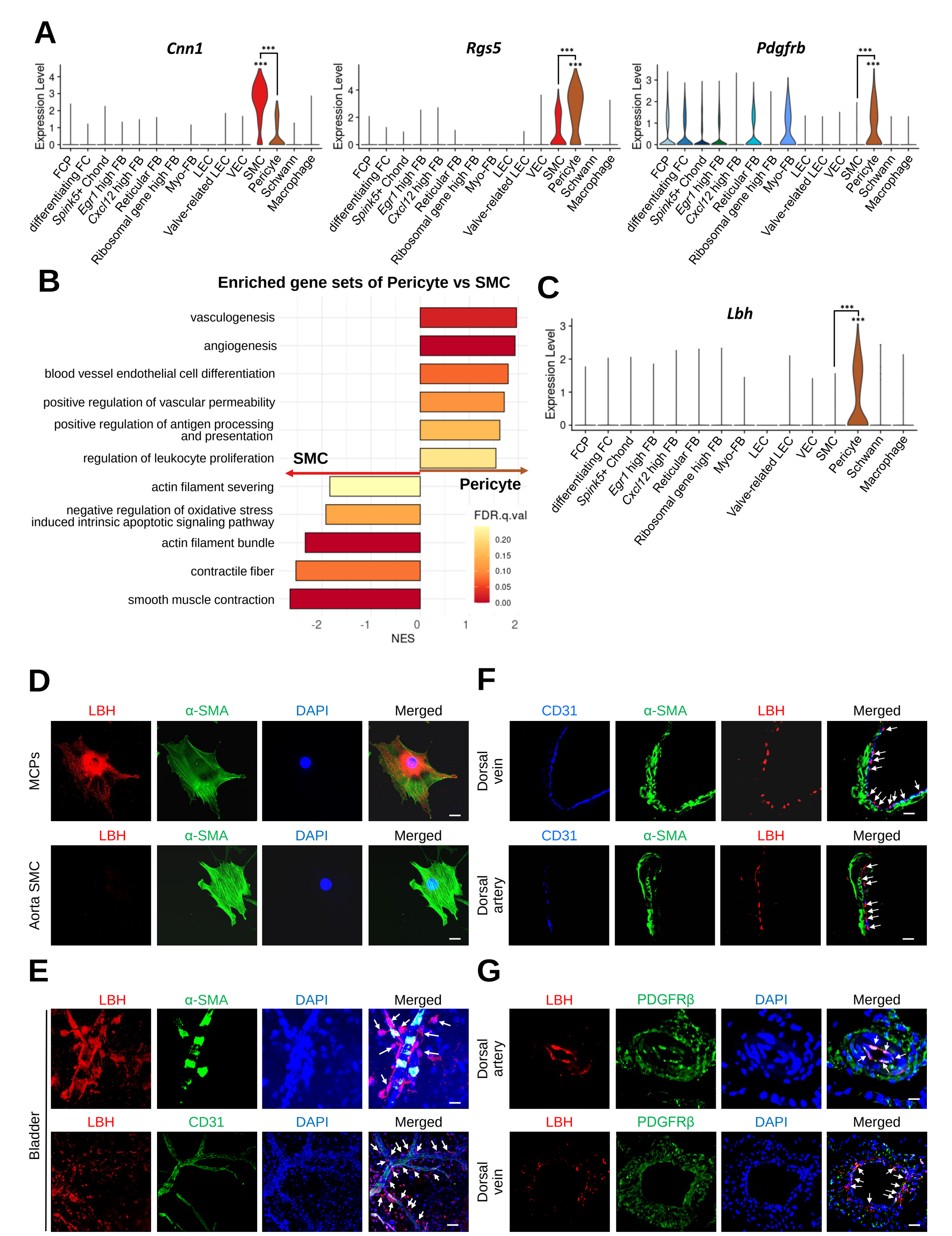
A
Cnn1
Rgs5
Pdgfrb
Expression Level
***
FCP
differentiating FC
Spink5+ Chond
Egr1 high FB
Cxcl12 high FB
Reticular FB
Ribosomal gene high FB
Myo-FB
LEC
Valve-related LEC
VEC
SMC
Pericyte
Schwann
Macrophage
B
Enriched gene sets of Pericyte vs SMC
vasculogenesis
angiogenesis
blood vessel endothelial cell differentiation
positive regulation of vascular permeability
positive regulation of antigen processing and presentation
regulation of leukocyte proliferation
actin filament severing
negative regulation of oxidative stress induced intrinsic apoptotic signaling pathway
actin filament bundle
contractile fiber
smooth muscle contraction
SMC
Pericyte
FDR.q.val
0.20
0.15
0.10
0.05
0.00
-2
-1
0
1
2
NES
C
Lbh
D
LBH
α-SMA
DAPI
Merged
MCPs
Aorta SMC
F
CD31
Dorsal vein
Dorsal artery
E
Bladder
G
PDGFRβ

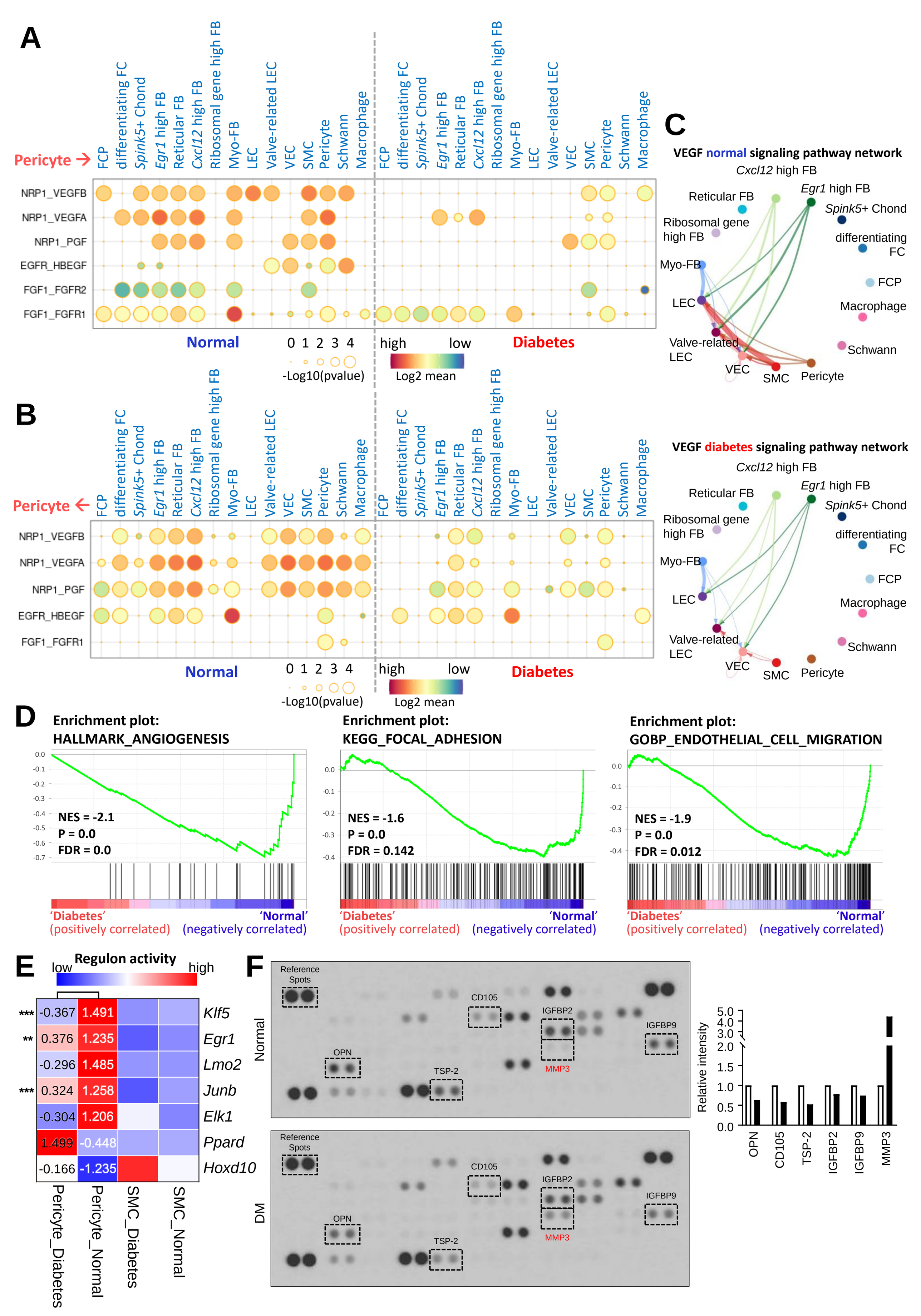
A
Pericyte →
FCP
differentiating FC
Spink5+ Chond
Egr1 high FB
Reticular FB
Cxcl12 high FB
Ribosomal gene high FB
Myo-FB
LEC
Valve-related LEC
VEC
SMC
Pericyte
Schwann
Macrophage
NRP1_VEGFB
NRP1_VEGFA
NRP1_PGF
EGFR_HBEGF
FGF1_FGFR2
FGF1_FGFR1
Normal
Diabetes
0 1 2 3 4
-Log10(pvalue)
high
low
Log2 mean
B
Pericyte ←
C
VEGF normal signaling pathway network
Cxcl12 high FB
Egr1 high FB
Reticular FB
Spink5+ Chond
Ribosomal gene high FB
differentiating FC
Myo-FB
FCP
LEC
Macrophage
Valve-related LEC
Schwann
VEC
SMC
Pericyte
VEGF diabetes signaling pathway network
D
Enrichment plot: HALLMARK_ANGIOGENESIS
NES = -2.1
P = 0.0
FDR = 0.0
Enrichment plot: KEGG_FOCAL_ADHESION
NES = -1.6
P = 0.0
FDR = 0.142
Enrichment plot: GOBP_ENDOTHELIAL_CELL_MIGRATION
NES = -1.9
P = 0.0
FDR = 0.012
'Diabetes' (positively correlated)
'Normal' (negatively correlated)
E
Regulon activity
low
high
*** -0.367 1.491 Klf5
** 0.376 1.235 Egr1
-0.296 1.485 Lmo2
*** 0.324 1.258 Junb
-0.304 1.206 Elk1
1.499 -0.448 Ppard
-0.166 -1.235 Hoxd10
Pericyte_Diabetes
Pericyte_Normal
SMC_Diabetes
SMC_Normal
F
Reference Spots
CD105
IGFBP2
IGFBP9
OPN
TSP-2
MMP3
Normal
DM
Relative intensity
5.0
4.0
3.0
2.0
1.5
1.0
0.5
0.0
OPN
CD105
TSP-2
IGFBP2
IGFBP9
MMP3

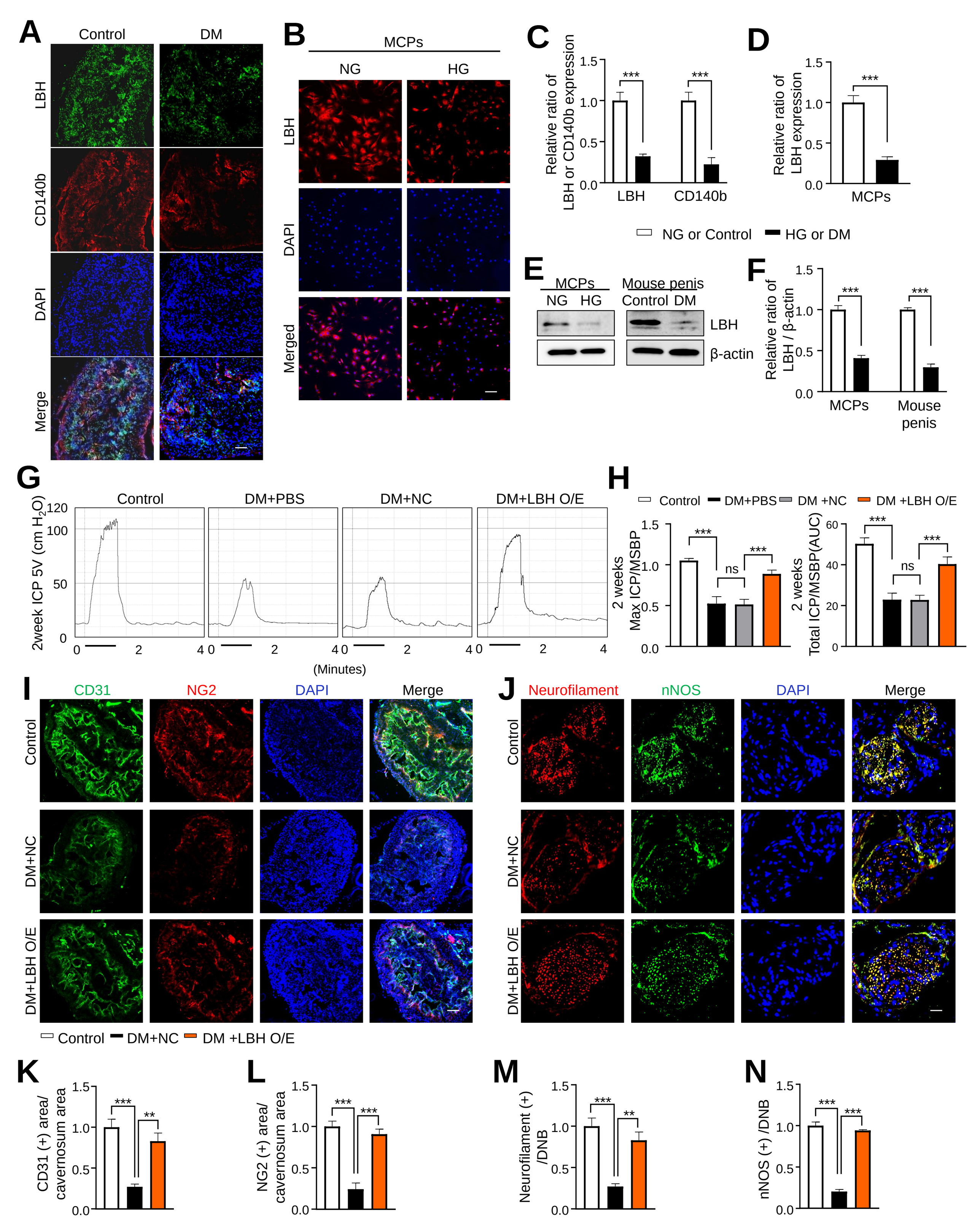
A
Control
DM
LBH
CD140b
DAPI
Merge
B
MCPs
NG
HG
LBH
DAPI
Merged
C
Relative ratio of LBH or CD140b expression
1.5
1.0
0.5
0.0
***
***
LBH
CD140b
D
Relative ratio of LBH expression
***
MCPs
NG or Control
HG or DM
E
MCPs
NG HG
Mouse penis
Control DM
LBH
β-actin
F
Relative ratio of LBH / β-actin
***
***
MCPs
Mouse penis
G
Control
DM+PBS
DM+NC
DM+LBH O/E
2week ICP 5V (cm H2O)
120
100
50
0
0 2 4
(Minutes)
H
Control
DM+PBS
DM +NC
DM +LBH O/E
2 weeks
Max ICP/MSBP
***
ns
***
2 weeks
Total ICP/MSBP(AUC)
60
40
20
0
***
ns
***
I
CD31
NG2
DAPI
Merge
Control
DM+NC
DM+LBH O/E
J
Neurofilament
nNOS
DAPI
Merge
Control
DM+NC
DM+LBH O/E
Control
DM+NC
DM +LBH O/E
K
CD31 (+) area/ cavernosum area
***
**
L
NG2 (+) area/ cavernosum area
***
***
M
Neurofilament (+) /DNB
***
**
N
nNOS (+) /DNB
***
***

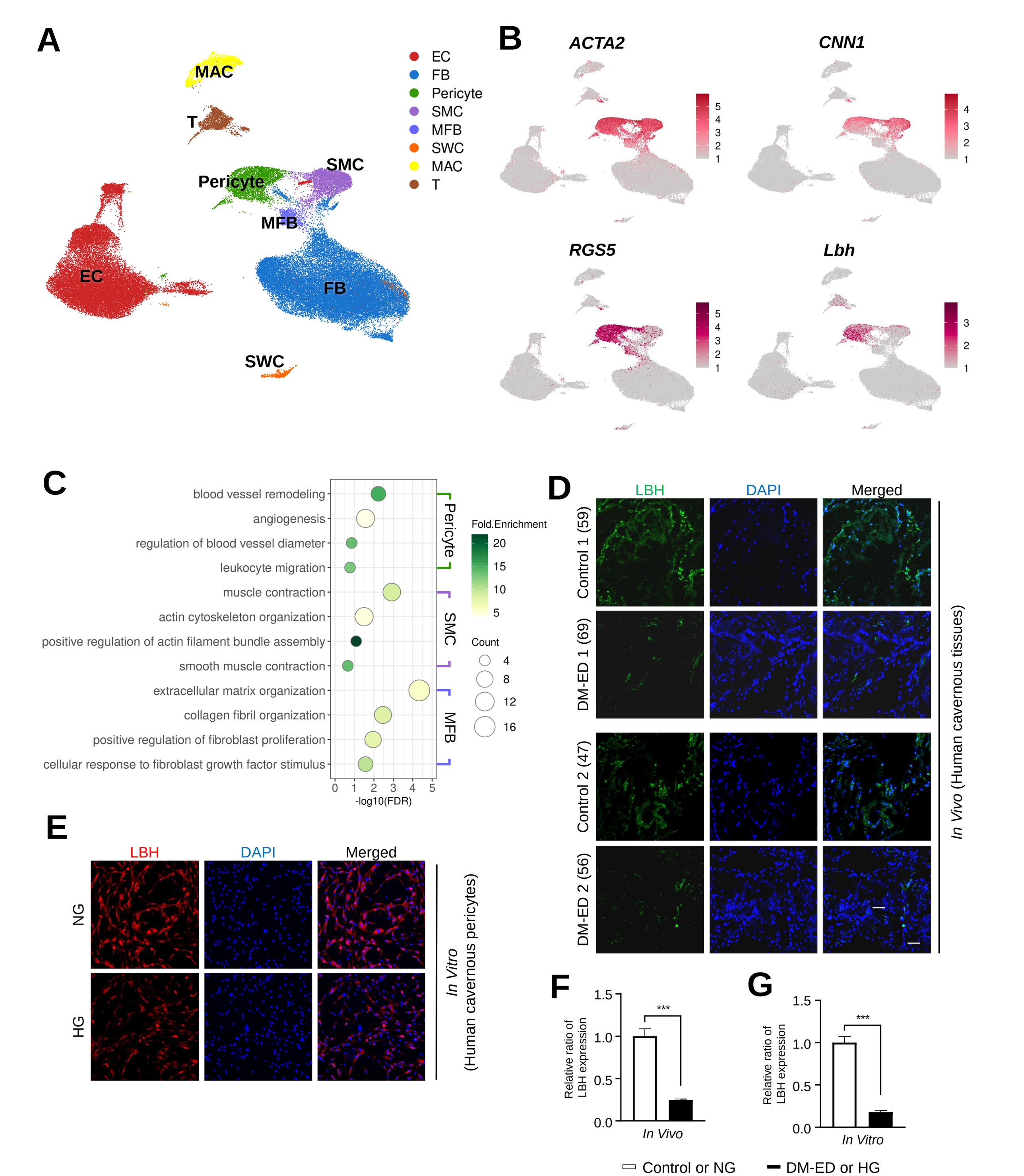
A
MAC
T
SMC
Pericyte
MFB
EC
FB
SWC
EC
FB
Pericyte
SMC
MFB
SWC
MAC
T
B
ACTA2
CNN1
RGS5
Lbh
C
blood vessel remodeling
angiogenesis
regulation of blood vessel diameter
leukocyte migration
muscle contraction
actin cytoskeleton organization
positive regulation of actin filament bundle assembly
smooth muscle contraction
extracellular matrix organization
collagen fibril organization
positive regulation of fibroblast proliferation
cellular response to fibroblast growth factor stimulus
-log10(FDR)
Pericyte
SMC
MFB
Fold.Enrichment
Count
D
LBH
DAPI
Merged
Control 1 (59)
DM-ED 1 (69)
Control 2 (47)
DM-ED 2 (56)
In Vivo (Human cavernous tissues)
E
LBH
DAPI
Merged
NG
HG
In Vitro (Human cavernous pericytes)
F
Relative ratio of LBH expression
In Vivo
G
Relative ratio of LBH expression
In Vitro
Control or NG
DM-ED or HG

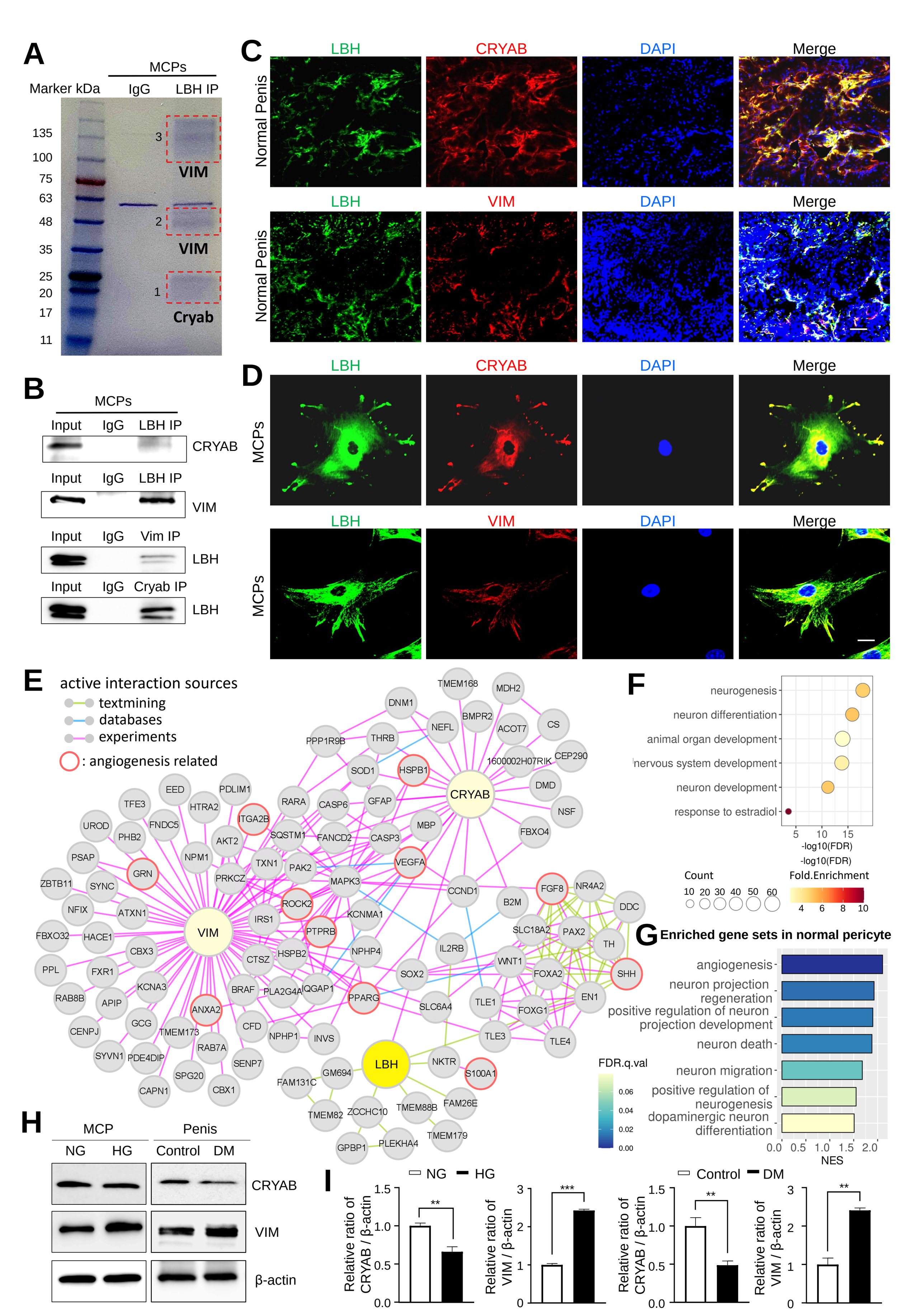
A
MCPs
Marker kDa
IgG
LBH IP
135
100
75
63
48
35
25
20
17
11
3
VIM
2
VIM
1
Cryab
B
MCPs
Input
IgG
LBH IP
CRYAB
Input
IgG
LBH IP
VIM
Input
IgG
Vim IP
LBH
Input
IgG
Cryab IP
LBH
C
LBH
CRYAB
DAPI
Merge
Normal Penis
LBH
VIM
DAPI
Merge
Normal Penis
D
LBH
CRYAB
DAPI
Merge
MCPs
LBH
VIM
DAPI
Merge
MCPs
E
active interaction sources
textmining
databases
experiments
: angiogenesis related
CRYAB
VIM
LBH
TMEM168
MDH2
DNM1
BMPR2
NEFL
ACOT7
CS
PPP1R9B
THRB
CEP290
1600002H07RIK
SOD1
HSPB1
DMD
EED
PDLIM1
TFE3
HTRA2
RARA
CASP6
GFAP
NSF
UROD
FNDC5
ITGA2B
PHB2
AKT2
SQSTM1
FANCD2
CASP3
MBP
FBXO4
PSAP
NPM1
TXN1
PAK2
VEGFA
GRN
PRKCZ
MAPK3
ZBTB11
SYNC
CCND1
FGF8
NR4A2
B2M
DDC
NFIX
ATXN1
ROCK2
KCNMA1
IRS1
FBXO32
HACE1
PTPRB
SLC18A2
PAX2
TH
CBX3
NPHP4
IL2RB
HSPB2
CTSZ
WNT1
PPL
FXR1
SOX2
FOXA2
SHH
KCNA3
BRAF
PLA2G4A
IQGAP1
RAB8B
APIP
PPARG
SLC6A4
TLE1
EN1
ANXA2
FOXG1
GCG
CFD
CENPJ
TMEM173
NPHP1
INVS
TLE3
TLE4
RAB7A
SYVN1
PDE4DIP
SENP7
NKTR
S100A1
SPG20
GM694
FAM131C
CAPN1
CBX1
TMEM82
ZCCHC10
TMEM88B
FAM26E
TMEM179
GPBP1
PLEKHA4
F
neurogenesis
neuron differentiation
animal organ development
nervous system development
neuron development
response to estradiol
5
10
15
-log10(FDR)
-log10(FDR)
Count
10 20 30 40 50 60
Fold.Enrichment
4 6 8 10
G
Enriched gene sets in normal pericyte
angiogenesis
neuron projection regeneration
positive regulation of neuron projection development
neuron death
neuron migration
positive regulation of neurogenesis
dopaminergic neuron differentiation
FDR.q.val
0.06
0.04
0.02
0.00
0.0 0.5 1.0 1.5 2.0
NES
H
MCP
Penis
NG
HG
Control
DM
CRYAB
VIM
β-actin
I
NG
HG
Relative ratio of CRYAB / β-actin
1.5
1.0
0.5
0.0
**
Relative ratio of VIM / β-actin
3
2
1
0
***
Control
DM
Relative ratio of CRYAB / β-actin
1.5
1.0
0.5
0.0
**
Relative ratio of VIM / β-actin
3
2
1
0
**